CHALMERS

Numerical modelling of paint curing in convective ovens

Master's thesis in Fraunhofer Chalmers Centre (FCC)

MADHAVAN VASUDEVAN

Numerical modelling of paint curing in convective ovens

MADHAVAN VASUDEVAN

Numerical modelling of paint curing in convective ovens
MADHAVAN VASUDEVAN

Numerical modelling of paint curing in convective ovens
Master's thesis in Fraunhofer Chalmers Centre (FCC)
MADHAVAN VASUDEVAN
Mechanics and Maritime Sciences
Fluid Dynamics
Chalmers University of Technology

Abstract

The paint application and the curing process is a crucial step in the automotive production lines as it accounts for both aesthetic appeal and protection against corrosion. The requirement of a standard for the paint curing process and quantification for improving performance parameters is the primary motivation for developing a mathematical model based on first principles. The complex curing process involves conjugate heat transfer, mass transfer and polymerization process. Extensive Three-Dimensional Computational Fluid Dynamics (CFD) based studies have been made in the literature with One-Dimensional mass transport modeling of the solvent at the paint layer-air interface with no resolution of heat transport within the same. Representative experiments of the curing process have been performed by Swerea-IVF and the measurements signify the importance of resolution of heat transport within the paint layer. The current study is intended to providing Heat Transfer Co-efficient (HTC) for the Three-Dimensional CFD simulations. The temporal resolution of the heat transport equation within the paint layer creates large separations of time scales and this makes the computational requirements in-feasible for the current scale of problem. A known value of HTC in the Three-dimensional CFD simulations provides an opportunity to avoid solving heat transfer in different phases simultaneously. Therefore, the current work is an attempt towards benefiting from both experiments and numerical techniques as One-Dimensional simulations have been developed to characterize the heat and mass transport within the paint layer to result in the optimized HTC based on the experimental measurements.

The work involved optimization of HTC in the heat transfer solver and a model parameter that represents evaporation at the paint layer-air interface in the mass transfer solver. It is observed in the work that the HTC is a weak function of concentration of solvent and the model parameter in the mass transport equation increased with decreasing concentration of the solvent. The model parameter in the mass transport equation increased with decreasing temperature to account for the reduction in diffusivity.

Keywords: Paint curing, One-Dimensional simulations, Optimization

ACKNOWLEDGEMENTS

English letters

Symbol	Description
a	Co-efficients in heat transfer equation
A	Area of cross section
b	Co-efficients in mass transfer equation
Bi	Biot Number
c_p	specific heat
C	Concentration
e_{rate}	evaporation rate parameter
f	distance ratio
h	thickness
J	Mass flux
l	length
P	Pressure
Q	Heat Energy transferred per unit time
q	Heat flux
S	source term
t	Time
T	Temperature
v	velocity
w	weight
x	Dimensional co-ordinate
X	Mass fraction (interchangeably used with C)
Y	Volume fraction

Subscripts

Symbol	Description
conv	Convective
e	East face
E	East node
exp	Experimental
i	Index position
Num	Numerical
w	West face
W	West node
P	Current cell node
res	resin
sat	Saturation
sol	solvent
x	Component along x direction

Superscripts

Symbol	Description
0	Previous time step
1	Current time step

Symbols

Symbol	Description
.	Dot product
$\overline{()}$	Averaged
$\in$	Belongs to

Greek letters

Symbol	Description
α	Activity of the solvent
$\hat{\eta}$	Generalized dimensional co-ordinate
κ	Thermal conductivity
ρ	Density
Δ	Difference
Δx	Cell size
δx	Node to node distance
ω	Specific turbulent dissipation rate
∇	Gradient operator

Units

Symbol	Description
s	Seconds
J	Joules
W	Watts
kg	Kilograms
m	metres
mm	millimeter
K	Kelvin
k	Turbulent kinetic Energy

Acronyms

CFD	Computational Fluid Dynamics
D	Diffusivity
-D	Dimensional
FDM	Finite Difference Method
FVM	Finite Volume Method
HTC	Heat Transfer Co-efficient
PDE	Partial Differential Equation
SST	Shear Stress Transport

CONTENTS

x

1 Introduction

The paint curing process like any other operations in the automotive industry, is a very complex problem. A wide variety of parameters could affect the quality of the paint and paint curing process. The paint application process is subjected to high levels of human interventions and therefore the possibilities of generation of defects are substantially high [3]. The high level of uncertainty also imposes a difficulty on proposing a standard for the process[19]. Therefore, predictions based on first principles will provide a standard to compare against for quality and thereby improve quality and performance parameters. The quality of the paint is of utmost importance as it does not only apply to the aesthetic appeal of the automobile but also act as a preventive anti-corrosive coating to the body on which it is painted [3]. The fundamental understanding of the process, apart from providing useful information regarding the performance parameters of the painted components, also provides opportunities to benefit in the industrial concerns. For example, the positioning of the automobile components inside the curing oven has been largely intuitive to provide the quickest curing and thereby incur minimum heating power supply to support the process. Similar concern is also applicable to the positioning of the inlet and exhaust fans. Improvement of curing cycle time through numerical modelling of continuous air flow in convective ovens has been one of the major focus of research in this field [9, 31] . Nowadays, the automotive production lines are extremely loaded to meet the heavy market requirements and it is hence not a practical idea to attempt to optimize these parameters in functional production lines. Therefore, demonstrative mathematical models are indispensable to represent the fundamental physics of the problem and provide useful information regarding opportunities to improve the process parameters [9, 10]. Also considering the pressing concern of impact of industrial operations on the environment, a scientific evaluation of sustainability of the processes is very important.

In reality, the painting process in the automotive industry involves paint application and curing alternatively for ideally 2-3 times. The curing process between two successive paint application process is to ensure that the paint applied in the successive processes do not diffuse together. Ideally the automobile parts or surfaces are thoroughly washed before paint applications to avoid defects [25]. The first application is usually the application of the electrocoat which is followed by the curing process. This is followed by a primer application and subsequent curing process. Finally, the base coat and the final coat are applied before the final curing process. Extensive analytical [12] [15] , numerical [9] [10] [12] and experimental [5] work have been performed in the field of paint curing process especially and also in the other processes involved in the overall painting operation. In regards to the paint application process, electrostatic spray painting was simulated using FVM based discretization in a dynamic catresean octree grid with a novel immersed boundary method which enabled modelling of moving objects without computationally expensive body conforming meshes by A.Mark et al. The efficient solving techniques helped simulating entire car bodies in few hours on a standard computer [2]. Numerical modelling using FVM based numerical calculation methodology for negative corona discharge for three species with application to externally charged power bells were developed by T.Johnson et al.[18]. In the work, numerical modelling of the corona discharge of three species was modelled in air and oxygen in wire cylinder and needle plane geometries. Higher order convective schemes were used in a cylindrical FVM framework in the work. An alternative method of modelling three species using domain decomposition method was developed by T Johnson et al. [29]. Also a simulation framework was established for coupled simulations of air flow by F. Edelvik et al., where the electrostatic fields and the charged paint particles were modelled as a part of the virtual paint factory project. The work also demonstrated that the same framework can be used to efficiently simulate the laydown of sealing or adhesive material [11].

In numerical modelling of paint curing process, it is of paramount significance to be able to utilize the appropriate models. A decision on level of resolution of scales determines the level of detailing that the results could provide. In principle, the model should provide a good balance between computational efforts and accuracy of the solution. The paint curing problem involves oven settings, physio-chemical characteristics of the paint material and the thermo-structural properties of the metal substrates on which the paint is applied[9]. The paint material consists of several distinct chemical species and the physio-chemical characteristics pertain to the impact on diffusivity of components of paint to diffuse within and out of the paint matrix as a result of increased temperature. Later, as the temperature of the painted surface is maintained at an elevated temperature for extended duration, the reminder of the paint matrix polymerizes to solid state as to what we observe as the painted automobile surfaces in our day-to-day lives. The overall paint curing process in reality includes the conjugate heat transfer, mass transfer and polymerization process on a phenomenological level [5] [10] [12] [15].

Therefore, a comprehensive paint curing model should demonstrate a sequential correlations of the under-

lying fundamental mechanisms as the following; Transient temperature history based on the oven settings, concentration of species in paint matrix and in the surrounding air as a consequence of increased temperature, fraction of conversion of remainder of paint matrix into polymerized state as a consequence of achieved temperature and concentration of species left in the paint matrix post diffusion. In addition to the heat transfer, mass transfer and the polymerization models developed to characterize the aforementioned mechanisms in the paint curing process, the qualitative characteristics are quantified using a network-structural model which assesses the structural performance of the polymerized matrix so formed by all other models [9]. In reality, as the oven gets warmed up, the evaporation process is usually completed in a span of 5-10 minutes and it is the polymerization process which takes a few hours to get completed. Therefore, it is logical to expect the polymerization process to predominantly affect the standard settings of the oven. In literature, rigorous empirical[10], numerical and experimental measurement techniques have been developed to estimate and optimize the curing characteristics from both physical[9] [6] [5]and chemical[4] standpoints. The aim of this work is to provide numerical calculations based information regarding the curing characteristics with the help of representative model parameters, which in turn are estimated from the experimental measurements. This nature of work therefore aims to bring in the benefit of both numerics and experiments and also bring down the time and expense to complete both of them.

In the interest of characterizing the paint materials thermo-chemically, predicting the temperature history and chemical composition of the paint through the curing process has been the prime focus of this work. The results of this work are aimed to aid the full-scale 3-D simulations where the aforementioned process parameters and geometrical framework involved in the paint curing are sought to be optimized. Therefore, the present work is aimed at developing a methodology to simultaneously represent heat and mass transfer in the paint curing process and obtain the values of useful model parameters through optimization, the knowledge of which is expected to reduce the computational burden on 3-D simulations. In the literature extensive studies have been made on analyzing the influence of macroscopic and microscopic properties on the settling process [12] [15] with resolution of transport properties in paint layer in 2-D and 3-D. On contrary, this study aims at maximizing models in the interest of reducing computational time and hence the impact of microscopic quantities are not resolved for characterizing the transport behaviour of paint components.

2 Theory

The mathematical modelling of paint curing process has been performed with varying levels of modelling and resolution in the literature, depending on the objectives of the work. Studying the settling process of the paint layers whilst curing[12] [15], optimizing the oven characteristics for an energy efficient curing process [9] [10], characterization of paint defects due to improper curing strategies [3][10][25] and identifying appropriate turbulence model[10] for the process has been the major topics of study. In the literature, the paint is typically modelled as a multi-component fluid with one volatile(solvent) and one non-volatile(resin) component [9] [10] [12] [15] [19]. In reality, as the painted substrate is heated, the solvent leaves to ambient air from the paint matrix in the vaporized form and thereby reduces the weight and thickness of the paint matrix. The evaporation process is largely controlled by the ambient air conditions and the diffusion within the paint layer. Although the conditions could alter the rate of evaporation, the end state of the paint matrix after the curing process by principle is invariant and equivalent to residual that is constituted by only the resin component. Appropriate reduction models need to be introduced for accounting the reduction in the thickness and weight of the paint layer.

2.1 Levelling motion of paint layers- A sub-macroscopic level insight

The fundamental physical properties which affect these macroscopic phenomena are surface-tension, viscosity, diffusivity and evaporation rate of the solvent. The surface tension of solvent and the resin are different. The non-volatile resin settles at the bottom on the substrate and the volatile solvent on the top of the coating. This settling behaviour leads to gradient in the concentration of the solvent or resin in the coating. The gradient thus also introduces a gradient in the surface tension within the coating film. The identification of surface-tension-gradient induced motion has been able to answer the "reversal" mechanisms in the paint curing process. The combined effect of surface tension induced force, surface-tension-gradient induced force, gravity and viscous forces characterize the levelling motion of paint layers in the curing process.

The nature of the surface tension force is to create an uniform level of coating and the gravity tends to move the fluid from thick to thin regions. The viscous force opposes the natural flow due to surface tension and gravity. The viscosity of the fluid keeps increasing until it eventually becomes a solid. It is also studied by [15], that the force induced by gravity in the simulation of leveling of paint layers is several orders less than that of the viscous, surface-tension induced and surface-tension-gradient induced forces. The inherent behaviour of the fluid to move from initially existing crests and troughs could be attributed to the surface tension dominated forces. These forces could not account for the continued motion of the fluid past the level surface to the reversed condition, but the surface-tension-gradient forces could. It is mentioned in the work by [12], that the surface tension induced and gravity induced forces reach a minimum when the intermediate level surface is achieved but the surface tension gradient induced forces has a very high value by then. In the particular work the concentration gradients along the coating height was neglected. This assumption justified a very high value of concentration difference which could lead to a high surface-tension-gradient induced force. Both the surface tension induced force and concentration difference fall to a very small value when a completely "reversed" situation is obtained. A subtle lag between the time when minimum concentration and minimum surface-tension-gradient indućed forces reached minimum values was accounted for the influence of gravity, viscous and the surface-tension induced forces. The subsequent amplitude of crests and troughs in the flow pattern keep reducing because of the increased viscosity of the paint, which is because of the increased concentration of resin in the paint. Along with the progress of the aforementioned processes, the average height of the coating layer keeps reducing because of the evaporation of the solvent.

2.2 1-Dimensional Forward Simulation Techniques

2.2.1 Modelling Heat Transfer

In the current work, both the heat transfer and mass transfer equations are solved transiently in 1-D, in the direction across the thickness of the paint layer. The cohesive effects in the paint matrix are not evaluated in the longitudinal and the transverse directions. The 1-D calculations of the mass diffusion in the paint layer is

studied through several methods in the literature. A non-dimensionalized transport equation is modelled by Domnick et al[10]. The non-dimensionalization was performed with respect to the changing thickness of the paint layer as the computational domain pertaining to paint and ambient surrounding dynamically change. In this work, moisture transport equation in the moving mesh reference frame was solved coupled with the unsteady heat transfer equation. The moving reference frame for mass transfer is to incorporate the shrinkage effects during the curing process. Whereas, the paint matrix is assumed as discrete slices using FDM by Lou et al[19] and the concentration diffusion, weight reduction calculations and thickness reduction are calculated sequentially by dedicated reduction models. Since the paint curing process is a moving mesh problem and as it is very transient in nature, scientific recommendations on the turbulence models to be used for 3-D simulations is very important. The Unsteady-RANS(U-RANS) with SST k-ω was adopted to be the most suitable choice as to give accurate heat transfer predictions with low grid sensitivity for complicated turbulent flow in the drying process [10].

The transport properties of both the heat transfer and the mass transfer mechanisms are largely influenced by the paint layer-air interface characteristics. For the heat transfer equation, the convection at the interface is described as the following.

$$\frac{q_{conv}}{A} = Q_{conv} = HTC(T_{int} - T_{air}) \tag{2.1}$$

The heat transfer equation does not account for the evaporative heat transfer and polymerization through a dedicated formulation. Although the relative influence of polymerization process when the evaporation is in progress is very minimal. This is unlike the models developed in the literature [5] [15] [10] [9], where the heat of vaporization explicitly formulated in the heat transfer solver. Since the evaporative heat transfer is a surface phenomenon, the idea is to represent the same using HTC. As could be seen from the Figure -2.1, 0.7mm thick steel plate and $46\mu m$ thick paint coating on it accounts for an average $10 - 20^oC$ difference of temperature. In the absence of a strong sink-like term in the heat transfer equation, the temperature distribution would attribute to unreasonable characteristics of the diffusion process. In a physical standpoint, q_{conv} amount of flux is withdrawn from the system continuously for accounting the phase change process in the paint layer by both evaporation and polymerization. This provides a balance to the system without which the temperature of the object will unrealistically keep increasing monotonically.
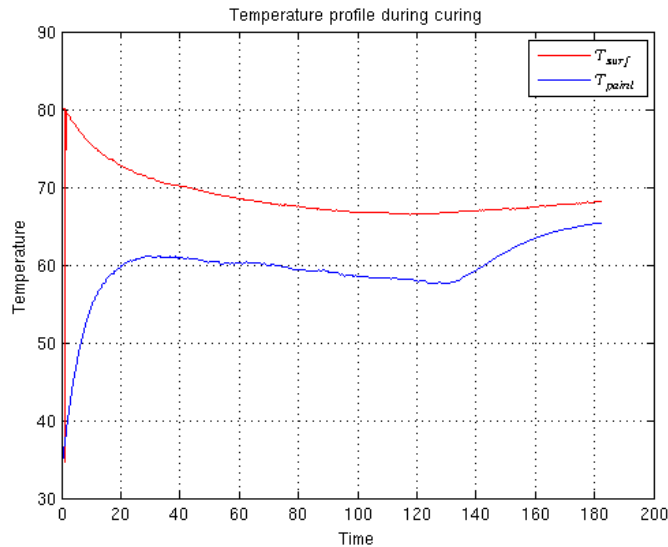

Figure 2.1: *Temperature distribution; The figure shows the variation of temperature on top of the paint layer and at the bottom of the metal surface on which the paint is applied. The data are obtained from experimental measurements*

2.2.2 Equations solved for heat transfer

The governing equation solved for the transient thermal distribution is the following.

$$\rho c_p \frac{DT}{Dt} = \nabla.(\kappa\nabla T) + S \tag{2.2}$$

where the gradient operator ∇ is defined as the following

$$\nabla = \frac{\partial}{\partial x}\hat{e_x} + \frac{\partial}{\partial y}\hat{e_y} + \frac{\partial}{\partial z}\hat{e_z} \tag{2.3}$$

The material derivative of a transport property could be defined as the following

$$\frac{D()}{Dt} = \frac{\partial()}{\partial t} + (V.\nabla()) \tag{2.4}$$

In the 1-D case with temperature as the transport property, the material derivative could be expressed as the following

$$\frac{DT}{Dt} = \frac{\partial T}{\partial t} + v_{rec}\frac{\partial T}{\partial x} \tag{2.5}$$

Considering the heat transfer to be dominant only across the thickness of the paint layer and incorporating the material derivative as defined, the representative 1-D heat equation for the problem is the following.

$$\rho c_p(\frac{\partial T}{\partial t} + v_{rec}\frac{\partial T}{\partial x}) = \frac{\partial}{\partial x}(\kappa\frac{\partial T}{\partial x}) + S \tag{2.6}$$

Detailed definition of v_{rec} is established along with the equations pertaining to mass transfer solver.

In the Equation -2.6, the velocity of mesh motion is considered as the convective velocity of temperature transport within the paint layer. Also it is important to note at this juncture that the dynamically changing domain regions pertain to only the paint layer. The metal substrate and heating plate are rigid and the material derivative in the metal regions could be expressed as the following

$$\frac{D()}{Dt} = \frac{\partial()}{\partial t} \tag{2.7}$$

As would be explained in the section on heat and mass transfer solvers section in methodology chapter, the solution of Equation -2.6 requires the knowledge of transport behaviour of the solvent and resin. Therefore, initial verification of the validity of the heat transfer solver is performed with only the heating plate and metal substrate. The solution algorithm pertaining to heat transfer within the paint layer is established after the heat transfer across only metal surfaces and mass transfer equation in the paint layer with constant temperature are established. In the current work, the heat conduction is assumed by simple Fourier's law as the following

$$Q = -\kappa A\frac{dT}{d\hat{n}} \tag{2.8}$$

Here, the term on the Left Hand Side (LHS) represents the transient term and the thermal capacity of the system. The first term on the right hand side represents the diffusion of heat by conduction and the last term represents a volume source/ sink of heat in the system. The sink term is modelled in the current work is alternatively replaced by an implicit boundary condition. From a physical standpoint, this approach is valid as convection is only a surface phenomenon. The numerical implementation using FVM is detailed in the methodology chapter.

2.2.3 Existing Models for Mass Transfer

For the mass transfer equation, the interface characteristics determines the rate of evaporation. As the evaporation depletes the concentration of solvent near the interface, the gradient in concentration across the thickness initiates and then propagates the mass diffusion of the solvent. At the end of every time step the mass fraction of solvent species in the immediate ambient air and corresponding changes in the paint matrix is evaluated and used as an initialization for the subsequent time-step calculations. The content of solvent in the ambient air acts as a dynamic Dirichlet boundary condition to the problem as the evaporation completes when all the moisture in the paint matrix enters the ambient air. The evaporation rate was estimated through the following equation [10]

$$P_{i,s}.\alpha_i(T, X_{i,j}) = P_{i,ph} \tag{2.9}$$

5

Here $P_{i,s}$ is the saturation pressure of every species in the paint matrix and α_i is the activity of the solvent that is dependent on the temperature and concentration of solvent and resin at the interface. $P_{i,ph}$ is the partial pressure in the air phase near the interface and this is interchangeably converted to mass fractions to act as a dynamic Dirichlet boundary condition for the concentration of solvent at the interface.

The interface concentration distribution is established as the following for assumption of transport discrete slices by FDM [19]

$$\rho_{res}h_{res}\frac{\partial Y}{\partial t} = K\frac{(P_a - \alpha P_{sa})}{P} + \rho_s D(X,T)\frac{\partial Y}{\partial x} \qquad (2.10)$$

Here, the p_{sa} is the saturation vapour pressure of the solver, p_a is the pressure in the air phase and P is the interface pressure. α is the activity of the solvent.

Although 3-D simulations have been performed, the mass diffusion across the paint layer has been studied through 1-D analysis by Fickian diffusion [5] [10] [19] , described as in the Equation- 2.11. Physio-chemical characteristics of the paint and amount of solvent already vaporized have been the major determining parameters in the literature[5] [10] [19] . In these works, the general formulation of diffusivity D within the paint matrix is adopted as the following.

$$J = -D\frac{\partial C}{\partial \hat{n}} \qquad (2.11)$$

$$D(X,T) = \eta e^{-((\gamma/X)+(E_d/RT))} \qquad (2.12)$$

Apart from characterizing the curing process, studies have also been done on optimizing the oven settings for reducing defects [10] and maximum energy efficiency [9]. The work by Dickie et al. unlike the other fundamental works establishing a model, has attempted to use an existing model to benefit from optimization. Since as mentioned in the introduction section, the moisture transport phenomena completes in the first 5-10 minutes of curing and the polymerization process takes longer duration to complete, the oven settings optimization has been performed based on the polymerization performance characteristics. In the work, a two stage oven has been tested with various heat input settings in consideration with fractional polymer conversion and maximum sheet metal temperature. This work is particularly of more interest for 3-D simulations than for the current 1-D simulations itself.

2.2.4   Current Model for Mass Transfer

As mentioned earlier, the pre-knowledge of involved properties of the paint materials are typically hard and hence a mathematical model that eliminated the requirement is the motive. However, the exact mathematical formulations with corresponding discretization of the sink term is detailed in the methodology section where the nature of the forward simulations are established. Other important reduction models and diffusivity models used in the simulations are detailed in the following

2.2.5   Equations solved for mass transfer

The nature of solution for the mass transfer equation is very synonymous with that of the heat transfer equation, as mathematically diffusion is the common mechanism governing both the phenomena. The vectorial form of mass transfer equation is the following

$$\frac{DX}{dt} = \nabla.(D\nabla X) + S \qquad (2.13)$$

Here again, the mass diffusion is predominantly found in the direction across the thickness of the paint layer and the representative transient 1-D mass transfer equation solved is the following.

$$\frac{DX}{Dt} = \frac{\partial}{\partial x}(D\frac{\partial X}{\partial x}) + S \qquad (2.14)$$

As for the Fourier's law of heat conduction for the heat transfer equation, the Fick's law as detailed earlier in the section is assumed for the concentration transport across the paint layers. Here D is the diffusivity of the concentration transport of the solvent. The diffusivity D of the concentration transport could be assumed as the following when the shrinkage in the layer is not accounted [16].

6

$$D = 0.6 \exp(\frac{-5300}{T}) \exp(\frac{-0.095}{X}) \tag{2.15}$$

And the diffusivity D in the paint could be assumed as the following when the shrinkage is accounted [16].

$$D = 0.43 \exp(\frac{-5300}{T}) \exp(\frac{-0.27}{X}) \tag{2.16}$$

The aforementioned definition of diffusivity D describes the direct dependence of the same on temperature. This means that the mass transfer equation is strongly coupled with the heat transfer equation. The definition of diffusivity D is theoretical as the value of diffusivity tends to approach 0 as the solvent concentration in the paint matrix approaches to 0. This makes the transport of solvent from the paint matrix decrease exponentially with time. Typically one would like to observe variation of complete transport behaviour in a finite duration of time and to suffice the requirement, following modification has been made.

$$D = 0.43 \exp(\frac{-5300}{T}) \exp(\frac{-0.27}{max(X, 0.1)}) \tag{2.17}$$

The modification means that a maximum of 10 percent correction has been provided to the theoretical diffusivity model.

As mentioned in the theory section, the solvent is volatile and it vaporizes during the curing process and the resin settles. The overall thickness and mass respectively of the multi-component fluid (paint) are defined as the following.

$$h_{tot} = h_{res} + h_{sol} \tag{2.18}$$

$$w_{tot} = w_{res} + w_{sol} \tag{2.19}$$

The mass due to resin is constant throughout the course of simulation and is also the expected residual at the end of the same. Consequently, the thickness due to resin is also constant it could be assumed as a hypothetical thickness of the paint matrix if it was constituted by no solvent. Similarly, this is the expected residual thickness expected at the end of the simulations. The concentration of the solvent in the paint is defined as the ratio of mass of the solvent in the paint matrix and the overall mass of the paint matrix. Alternatively, concentration of the resin in the paint is defined as the ratio of mass of the resin in the paint matrix and the overall mass of the paint matrix.

$$X_{sol} = X = \frac{w_{sol}}{w_{sol} + w_{res}} \tag{2.20}$$

$$X_{res} = \frac{w_{res}}{w_{sol} + w_{res}} \tag{2.21}$$

Similarly, the volume fraction of the solvent and the resin are defined as the following

$$Y_{sol} = Y = \frac{v_{sol}}{v_{sol} + v_{res}} \tag{2.22}$$

$$Y_{res} = \frac{v_{res}}{v_{sol} + v_{res}} \tag{2.23}$$

At every time step until when all the air has evaporated in the ambient surroundings, there is a continuous reduction in weight and thickness as the solvent moves out of the paint matrix. The concentration of the solvent is evaluated in every computational cell. With the known mass of resin and evaluated concentrations, the overall mass of the paint matrix and mass of solvent could be computed. The ratio of thickness constituted due to solvent or resin represents the volume ratio as the problem solved is 1-D in nature. The volume ratios and mass fractions are interchangeably computed using the following relationship.

$$Y_{sol} = \frac{X_{sol}}{X_{sol} + (1 - x_{sol})\frac{\rho_{sol}}{\rho_{res}}} \tag{2.24}$$

With a known value of volume fractions and a constant resin constituted thickness, the thickness constituted due to solvent could be estimated. The overall reduction in the thickness of the paint layer is evaluated as the sum of reduction in thickness due to solvent in all the computational cells.

$$h_{red} = \sum_{cells} h_{i,prev} - \sum_{cells} h_{i,curr} \tag{2.25}$$

The reduction in thickness with incorporating corrections, Equation-2.17 will be considered to Equations-2.15 and 2.16 for the diffusivity D model. Two, considering the deformation of the mesh, the material derivative of properties need to be established, the transport equation is expressed as the following

$$\frac{\partial X}{\partial t} + v_{rec} \frac{\partial X}{\partial x} = \frac{\partial}{\partial x}(D \frac{\partial X}{\partial x}) + S \tag{2.26}$$

The velocity v_{rec} is defined as the reduction of thickness of paint matrix per unit time step considered.

$$V = v_{rec} = \frac{h_{red}}{\Delta t} \tag{2.27}$$

As mentioned for the heat transfer, the numerical implementation of the mass transfer using FVM is detailed in the methodology chapter. And the numerical implementation of all the equations and the optimization process in the current work is carried out in *Matlab*

3 Simulation Strategies

The benefit of Immersed Boundary Methods(IBM) [1] [21] [22] is that, the fluid containing cells are represented by Eulerean approach while the immersed boundary of a moving object is described by a Lagrangian representation. These representations are coupled by Immersed boundary conditions that force the fluid to follow the boundaries of the immersed object. There are several techniques in the literature to implement the immersed boundary condition and the most effective of them have been mirroring method and mirroring and extrapolating method suggested by Mark et al[21]. Also a deviation and validation of a novel second accurate order implicit immersed boundary method was implemented by Mark et al[1]. In reference to the current work, paint curing process as well includes the moving mesh problem where, as the thickness of the paint layer reduces transiently and the ambient air replaces the domain regions that were previously occupied by the paint matrix. Therefore, an efficient numerical solver that handles moving mesh flows is necessary to carry out the 3-D simulations that are to follow the current work in the thesis.

3.1 IBOFlow

IBOFlow (Immersed Boundary Octree Flow Solver) is an in-compressible Finite Volume Method (FVM) discretization based fluid solver. The pressure and velocity fields are coupled using the SIMPLEC (Semi-Implicit Method for Pressure Linked Equations-Consistent) technique. The Cartesian octree grid could be dynamically refined to follow moving bodies. The collocated grid configuration is used to store the variables and Rhie and Chow (1983) interpolation techniques are used for the pressure fields to avoid checker-board oscillations of the pressure and velocity fields. Also the existing implementation of multi-objective optimization of heat sink design using Sandwiching Algorithm and Immersed boundary boundary CHT solver[27, 20] by T. Andersson et al, in IBOFlow. The work done by F. Svelander et al[26], is used to calculate the volume and area fractions used in the CHT solver. The solver has previously been used to predict 3D bioprinting [14] and jetting of solder paste on electronic devices with mixed wettablities [13].

3.2 1-D Simulations

The paint curing process involves conjugate heat transfer where the metal substrate undergoes a solid state conduction and ambient air undergoes convection. Historically, conjugate heat transfer has been the effective mathematical method where the heat transport in the solid domain and flow domain are solved separately and the temperature and flux across the interface is evaluated using simultaneous boundary conditions. This method has been effective in most realistic cases where the HTC at the interface is not known. Characterizing convective heat transfer by means of defining the HTC has been very successful modelling techniques where the definition of HTC through empirical correlations have been possible to made. On the other hand, this technique also posses a difficulty that theoretical characterization of convective heat transfer inevitably requires the knowledge of HTC to couple the transport of heat across the interface.

The thickness of the metal substrate generally is of few orders of magnitude larger than that of the paint layer. This in turn reflects on the separation of time scales of conduction in the metal substrate and in the paint layers. A practical temporal refinement for the heat conduction in the metal surface will not be suitable for the heat conduction in the paint layer. These large time scales will miss out on the heat transport within the paint layer and just reflect as, that the top layer of the paint reaches the temperature that is achieved in bottom layer without any time delay. And if the temporal discretization of the 3-D CFD simulations are performed with the time scales pertaining to the heat diffusion in the paint layer, then the computational requirements are impractical to meet considering the full scale of the problem. Therefore, the utilization of conjugate heat transfer technique is particularly not an appropriate approach for the paint curing process especially. In the work done by Lou et al, Domnick et al and Blanc et al the temperature gradient across the paint layer has been neglected. This has been motivated by low Biot Number achieved in the paint layer. As the Biot Number is the ratio of the resistance offered by the conductive heat transfer to the convective heat transfer, all the heat flux flows across the paint layer without any effect. The Biot Number is defined as the following.

$$Bi = \frac{hl_c}{k} \tag{3.1}$$

Representative experimental measurements have been performed by Swerea-IVF and the measurements suggest that the temperature resolution across the paint layer is crucial. This led to an alternative approach to estimate the HTC and thereby drastically reduce the computational time. By this way, the HTC at the interface of the solid and the fluid is provided to the simulation as a pre-determined value which is a function of concentration and temperature. HTC is usually affected by several factors like temperature, concentration of species in the paint matrix, concentration of species in the ambient air and velocity of air. In the present work, the characterization of the HTC is performed with an assumption that the temperature of the paint layer and the concentration of species in the paint layer are the dominant parameters influencing the same.

Mathematically at this stage, HTC is expressed as the following.

$$HTC = HTC(C) \tag{3.2}$$

Where C denotes the concentration of species and dependence of concentration achieved on temperature at different time instances is explained in the sections to follow. The establishment of strong dependence of concentration of species on temperature in turn creates a functional dependence for the HTC and is expressed as the following,

$$HTC = HTC(C(T)) \equiv HTC = HTC(C,T) \tag{3.3}$$

In the 3-D simulations, the paint layer region will not be resolved for the heat transfer solver but only for the mass transfer solver. It is also interesting to note that the choice of solving 1-D mass transfer equation in the full scale 3-D CFD simulations is feasible option as the time scales of mass diffusion is much are larger to that compared of the heat diffusion and hence could be matched with that of the overall 3D simulations. The mass transfer solver will provide concentration values for which corresponding pre-determined HTC values from the 1-D heat transfer solver will be provided to the 3-D solver. In principle, the 1-D simulations not only provide useful information on nature of results to expect from the 3-D simulations but is also useful to reduce the computational efforts of the same.

4 Experimental Measurements

The experimental measurements for the current work have been made by Swerea- IVF. Two different sets of measurements have been performed. The experiments were aimed at recording the values of transient residual weight and temperature achieved in the paint matrix over the paint curing duration.

4.1 Weight reduction

The weight reduction has been measured for at four different temperatures, 313, 323, 333 and 343K for both the Imron white[8] and Imron silver paint[7] material over the duration of curing. It is assumed that the solvent contained in both the paint materials is water. From the initial and the final weights of the paint matrix, the initial composition of the resin and the solvent are evaluated. Further, the density of the resin and initial thickness of the paint layer are evaluated through the Equations -2.18, 2.20 and 2.24. The obtained values have been tabulated in the Tables- 4.1 and 4.2 for Imron white and Imron silver respectively. This experiment is performed by initially spraying the paint materials manually into an aluminium cup which is 100mm in diameter and allowing it to get cured at the aforementioned constant temperatures and measuring the sample weights at various instants in time. The following plot shows the weight reduction of the four different samples at four different temperatures for Imron white and Imron silver respectively. At first, faster evaporation of solvent in Imron silver paint at lower temperatures compared to that at higher temperatures could represent unphysical characteristics of diffusion as the mass diffusion is always accelerated at higher temperatures. However, obtaining the values of initial thickness revealed that the samples at higher temperature that took longer duration were started for curing from increased initial thickness.
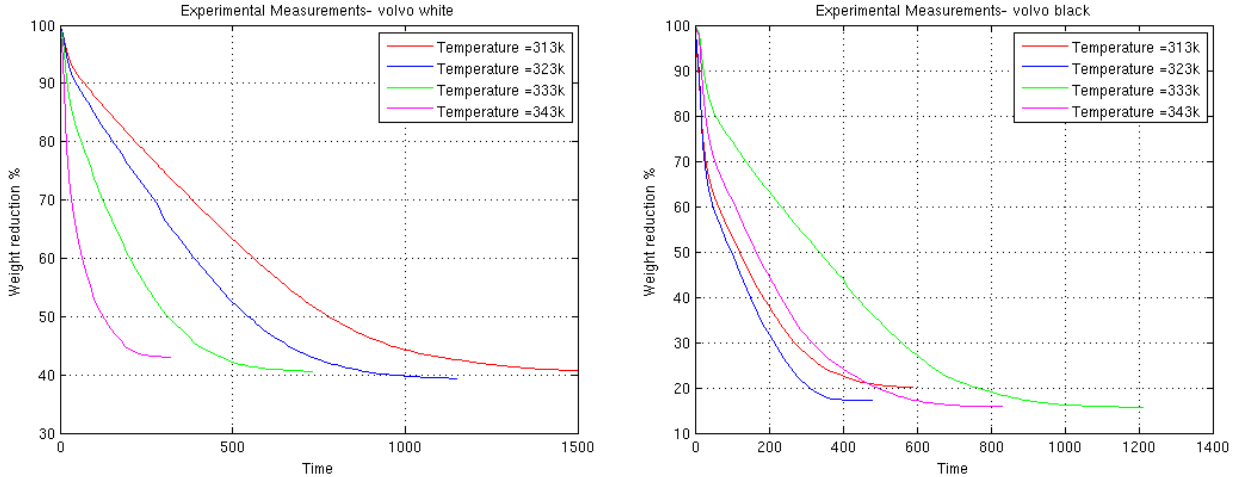

Figure 4.1: *Experimentally measured weight reduction curves for Imron white and Imron silver at 313, 323, 333 and 343K*

Table 4.1: Reference experimental measurement data for Imron white paint

Temperature (k)	Initial Weight (g)	Concentration of resin	Initial Thickness (1e-4)m	$\rho_{res}(kg/m^3)$
313	1.391	39.41	1.073	2650
323	1.606	40.76	1.121	2688
333	1.225	40.64	0.925	2684
343	1.5908	38.87	1.2382	2635

The density of the Imron white and Imron silver for calculations is assumed as their respective means obtained, $2664kg/m^3$ and $2215kg/m^3$.

Table 4.2: Reference experimental measurement data for Imron silver paint

Temperature (k)	Initial Weight (g)	Concentration of resin	Initial Thickness (1e-4)m	$\rho_{res}(kg/m^3)$
313	0.624	20.19	0.634	2253
323	0.806	17.12	0.850	2260
333	2.148	15.74	2.344	2186
343	1.758	15.81	1.8845	2187

4.2 Temperature Measurements

The experiment is conducted by placing a painted(wet) metal surface on a heating plate in such a way that the heating plate is not completely covered by the painted plate. For the temperature distribution, the temperature is measured at two different locations in the domain. The thermocamera has access to capture the temperature at the top of the painted surface and top of the heating plate/ bottom of the metal substrate. The data available for surface painted with Imron white and Imron silver are provided in the Figure -4.2. In the particular numerical study where the optimization of HTC was performed with the following temperature profiles as the reference, an emissivity of 0.95 unity is assumed for both the heating plate and 0.91 for the painted metal substrate.
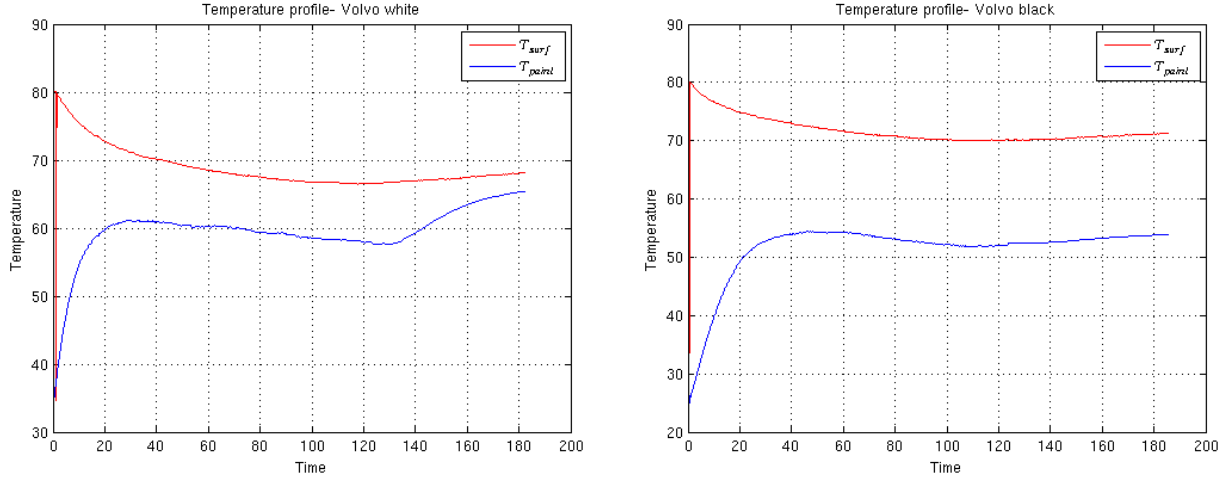

Figure 4.2: *Experimentally measured temperature profiles for Imron white and Imron silver at the top of the paint layer and bottom of the metal substrate*

5 Methodology

As mentioned in the theory sections, to avoid the dependence on very involved theoretical parameters for modelling the paint curing process, the current study is focused on developing a very simple mathematical model which is steered by means of optimizing two different model parameters in heat transfer and mass transfer equations; one in each equation. Effectively, only the evaporation phase of of the paint curing is aimed to be modelled. The HTC implicitly accounts for the latent heat of vaporization and hence no additional modelling of the heat transfer through vaporization is performed. In the mass transfer equation, the evaporation is controlled by a model evaporation rate parameter, e_{rate}. This model parameter is used to characteristically represent the evaporation instead of the traditional way[5][9][10] by pressure distributions at the interface and physio-chemical properties of the paint material. The evaporation rate parameter is modelled with a linear dependence on the concentration of solvent at the paint layer-air interface. A non-linear modelling of the evaporation rate parameter with the interface solvent concentration as in the Equation -5.28 is expected to be provide more realistic characterization of the solvent transport[12]. Such a definition of evaporation rate parameter is also expected to help reduce or eliminate the correction provided to the definition of diffusivity used. The definition and correction of diffusivity used pertain to the descriptions in the theory chapter.

It is to be noted at this juncture that neither the HTC value in the heat transfer equation, nor the e_{rate} evaporation rate parameter in the mass transfer equation is known. This introduces the necessity of solving an inverse problem. The inverse problems are a class of mathematical problems where the results of the problem are known but the causes corresponding to the results are not known. In reference to the context of the current problem, experimental measurements have been made to assess the heat and mass transfer characteristics of the paint layer. Temporal variation of the temperature distribution and weight reduction of the paint matrix are known from the experimental measurements. The HTC and the evaporation rate parameter that caused the aforementioned temperature and weight reduction are hence considered as estimated parameters. The HTC and evaporation rate parameter are evaluated using optimization process with experimental measurements as the reference values. This is a very generic and qualitative approach in principle as the methodology could be utilized for problems with similar characterizing physics.

In the following subsections, the fundamentals of 1-D heat transfer and 1-D mass transfer solver are detailed. The validity of the solvers developed are also explained by demonstrating the results with different boundary condition. The subsections are to be viewed as to provide only qualitative description of results and not the exact results only. These model results are used to optimize parameters as mentioned earlier and methods adopted for optimization are to follow in the subsequent chapter.

5.1 Heat Transfer without Paint Layer

As solving heat transfer across the thickness of the paint layer requires the knowledge of solutions of mass transfer equations solved simultaneously across the same paint layer, the basic validation of the heat transfer solver is performed by analyzing the heat transfer across the heating plate and metal substrate, thereby eliminating the paint layer. The transient 1-D heat transfer equation solved for the domains pertaining to the metal substrate and heating plate is the following

$$\rho c_p \frac{\partial T}{\partial t} = \frac{\partial}{\partial x}(\kappa \frac{\partial T}{\partial x}) + S \tag{5.1}$$

The heat transfer equation is discretized using Finite Volume Method (FVM) techniques as the following.

$$\int_{\Delta t} \int_{\Delta x} \rho c_p \frac{\partial T}{\partial t} dx dt = \int_{\Delta t} \int_{\Delta x} \frac{\partial}{\partial x}(k \frac{\partial T}{\partial x}) dx dt + \int_{\Delta t} \int_{\Delta x} S dx dt \tag{5.2}$$

$$\rho c_p \Delta x (T_p^1 - T_p^0) = ((k \frac{\partial T}{\partial x})_e - (k \frac{\partial T}{\partial x})_w) \Delta t + \overline{S} \Delta t \Delta x \tag{5.3}$$

Here, the subscripts e and w refer to the values at the east and west faces of the cell where the fluxes are evaluated. The superscripts 0 and 1 represent that the value are from previous and current time step respectively. $\overline{S}$ represents the volume averaged value of the source term.

$$\rho c_p \Delta x \frac{T_p^1 - T_p^0}{\Delta t} = (k_e \frac{T_E - T_P}{\delta x_e}) - (k_w \frac{T_P - T_W}{\delta x_w}) + \overline{S} \Delta x \tag{5.4}$$

The subscripts P represents the value at the current cell node for which the computation is performed. The subscripts E and W represents the values at the neighbouring cell nodes in the corresponding east and west directions. Δx represents the size of the 1-D cell and the δ_e and δ_w are the cells node-to-node distance in the east and the west directions respectively.

Physical properties (say β) at the faces of the cells have been assumed through linear interpolation of cell centre values of the two adjacent cells.

$$\beta_e = \beta_P(1 - f_e) + \beta_E(f_e) \tag{5.5}$$

$$\beta_w = \beta_P(1 - f_w) + \beta_W(f_w) \tag{5.6}$$

where the distance ratios f_e and f_w are defined as the following

$$f_e = \frac{\Delta x/2}{\delta x_e}; f_w = \frac{\Delta x/2}{\delta x_w} \tag{5.7}$$

The equations have been implicitly solved and hence the temperature values in the neighbouring nodes in the spatial discretization have been considered from the time step same as the equation is being solved for. Therefore, the discretized heat transfer equation takes the following form.

$$a_p T_p^1 + a_e T_E^1 + a_w T_W^1 = a_p^0 T_P^0 + b \tag{5.8}$$

$$a_p^0 = \rho c_p \frac{\Delta x}{\Delta t}; b = \overline{S}\Delta x \tag{5.9}$$

$$a_e = -\frac{k_e}{\delta x_e}; a_w = -\frac{k_w}{\delta x_w} \tag{5.10}$$

$$a_p = a_p^0 - a_e - a_w \tag{5.11}$$

5.1.1 Implicit Boundary Conditions

In the transient solver, two boundary conditions are required to be defined. One at the bottom of the heating plate and one at the top of the metal surface and at the bottom of the heating plate, a perfect insulation is modelled with no heat flux leaving the system. At the top of the metal substrate, the convective heat transfer is modelled as in the Equation -2.1. Since convective heat transfer is a surface phenomena, the sink like term could be alternatively be defined using an implicit boundary condition by prescribing a negative flux. The following description is intended to demonstrate the ways to introduce implicit boundary for different boundary conditions with the help of ghost cells.

If Dirichlet boundary condition is applied in the east boundary, discretization is performed as the following in the concerned boundary

$$a_g = a_e \tag{5.12}$$

$$a_{p,corr} = a_p - a_g \tag{5.13}$$

$$b_{corr} = b - 2(C)a_g \tag{5.14}$$

If Neumann boundary condition is applied in the east boundary, discretization is performed as the following in the concerned boundary

$$a_g = a_e \tag{5.15}$$

$$a_{p,corr} = a_p + a_g \tag{5.16}$$

$$b_{corr} = b - (\Delta x)(C)a_g \tag{5.17}$$

Here, C in the first and the second case hold the value of the Dirichlet and Nuemann value specified as the boundary conditions.

5.1.2 Verification of Heat Transfer Solver

Before the implementation of the coupled heat and mass transfer solvers, the results of 1-D transient heat transfer solver were verified with a variety of boundary conditions and the convergence trends were analyzed. The input parameters for the transient 1-D heat transfer solver used for all simulations in general have been summarized in Table- 5.1.

Table 5.1: Constants and values; Heat Transfer equation - Thin plates

Physical property/ constants	Values
HTC (assumed/ to be corrected)	450 W/m^2k
T$_{ref}$	298k
Thickness of Aluminum plate	0.7mm
Thickness of Copper plate	0.7mm
Source	25000 W/m^2 (only for Nuemann-Nuemann)
k$_{Al}$	237 Wm/k
k$_{Cu}$	401 Wm/k
rho$_{Al}$	2712 kg/m^3
rho$_{Cu}$	8940 kg/m^3
c$_{p,Al}$	910 J/kg k
c$_{p,Cu}$	390 J/kg k
Total simulation time	2s (Dirichlet- Dirichlet and Dirichlet-Nuemann)

Dirichlet -Dirichlet

The initial state is known and the boundary conditions at the ends of the plate are prescribed with fixed temperatures, in this case 315k and 298k. This is typically the simplest combination of boundary conditions but in reality it is hard to know the specific boundary values at both the ends. In our context it pertains to the bottom of the heating plate and the top of metal substrate. The results pertaining to this combination of boundary conditions are as in the Figure -5.1. The convergence study shows the maximum difference of temperature corresponding to any node in the domain between the previous and the subsequent time steps.
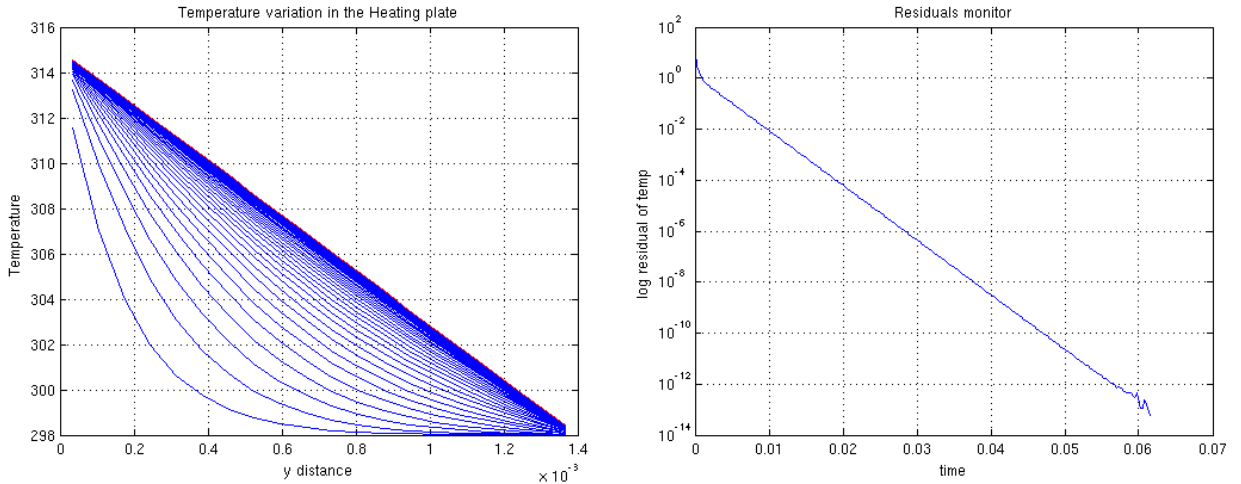

Figure 5.1: *Temperature evolution in time and convergence study with Dirichlet-Dirichlet case*

A time-step independence and grid independence study is performed to motivate the selection of number of time steps and number of cells in the metal substrate and heating plate for further studies in the implementation of coupled heat and mass transfer solver and optimization. The results show that 5 cells with a minimum 5 time steps is sufficient to reach to a convergent solution. The value of minimum Δt required for convergence could alternatively be described from the time step convergence. The aim here is to prove that it is sufficient to discretize with practically large Δt according to cases as the nature of the PDE and boundary conditions are

simple. Also since the solutions become convergent with large time steps, they are not suitable for comparing transient solutions and therefore the steady state solutions have been compared for all the 3 different boundary condition cases for the heat transfer solver.
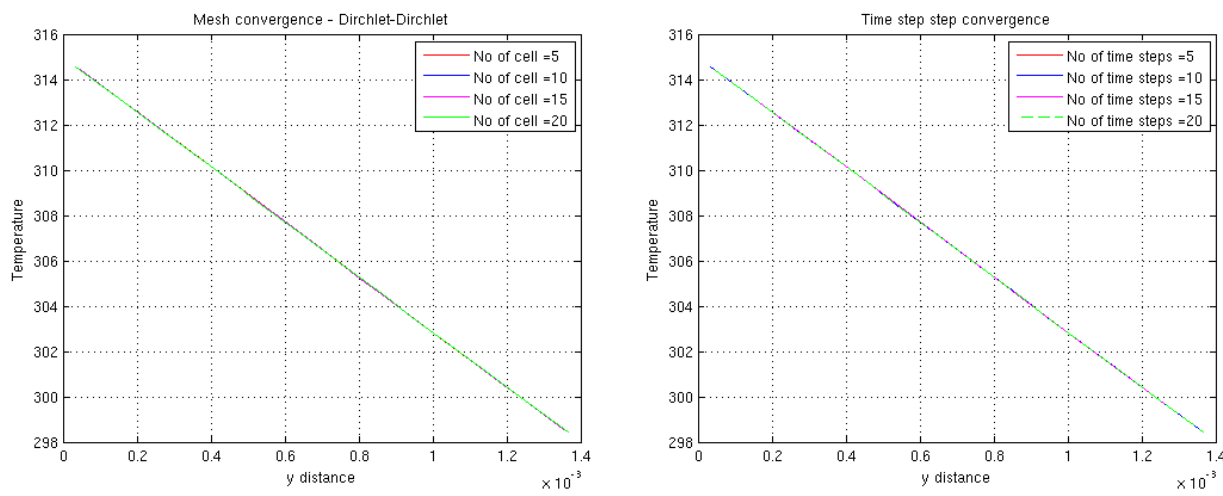

Figure 5.2: *Mesh convergence and time step independence study for Neumann-Neumann case*

Dirichlet - Neumann with convection

The initial condition is known and the temperature in one of the ends is known and the flux of heat transfer is known through the other end of the plate. This typically means that the temperature at the bottom of the copper heating plate is known and the flux at the metal substrate-air is known. The results pertaining to this combination of boundary condition are as in the Figure - 5.3. In the given problem, the prescribed temperature on side of the metal substrate limits the transient rise of temperature on the boundary with metal substrate- air interface. Also the convective heat transfer prescribed through the implicit boundary condition acts as a sink.
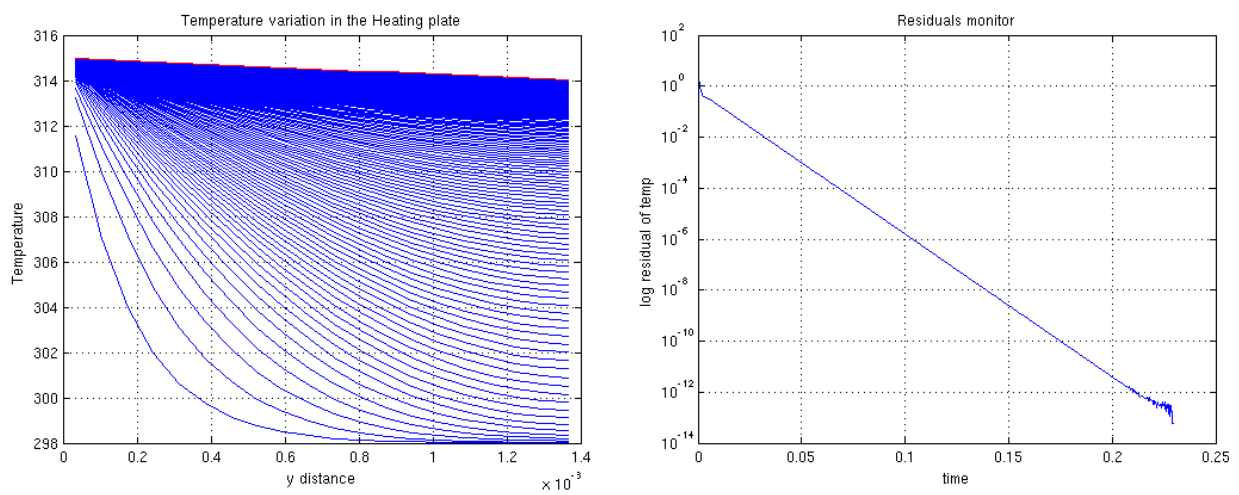

Figure 5.3: *Temperature and convergence study with Dirichlet-Neumann case*

As a similar grid and time-step convergence study has been made as in the Dirichlet-Dirichlet case. As since the nature of PDE and the boundary conditions are simple, the combination of the boundary condition also required only 5 cells with minimum of 5 time steps.
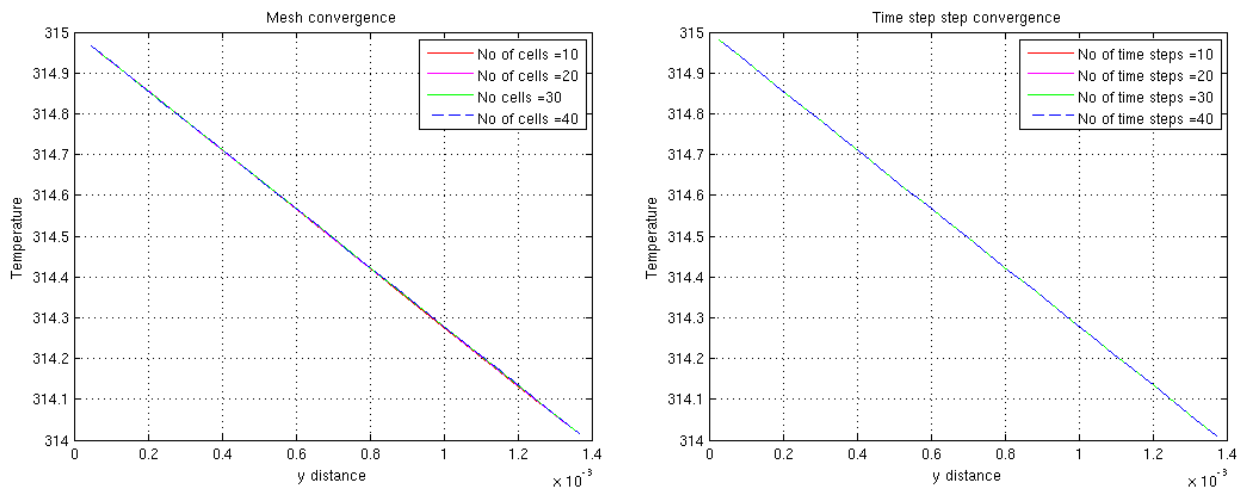
Figure 5.4: *Mesh convergence and time step independence study for Neumann-Neumann case*

Neumann- Neumann with Convection

This combination of boundary condition is not used for the further studies but it is of interest to show the validity of the solver as this is one of the most realistic combination of boundary conditions. In this special case, a heating source considered is modelled in a heating plate over which the metal substrate is modelled. The convective heat transfer to the ambient surroundings from surface in contact with ambient air reduces the surface temperature. The convective heat transfer again acts as a sink through the boundary condition by controlling the temperature rise, thereby allowing the system to settle with a steady state values in time. The results for the same are as in the Figure-5.5. Perhaps, it is important at this stage to note that the HTC value used is an assumed value.
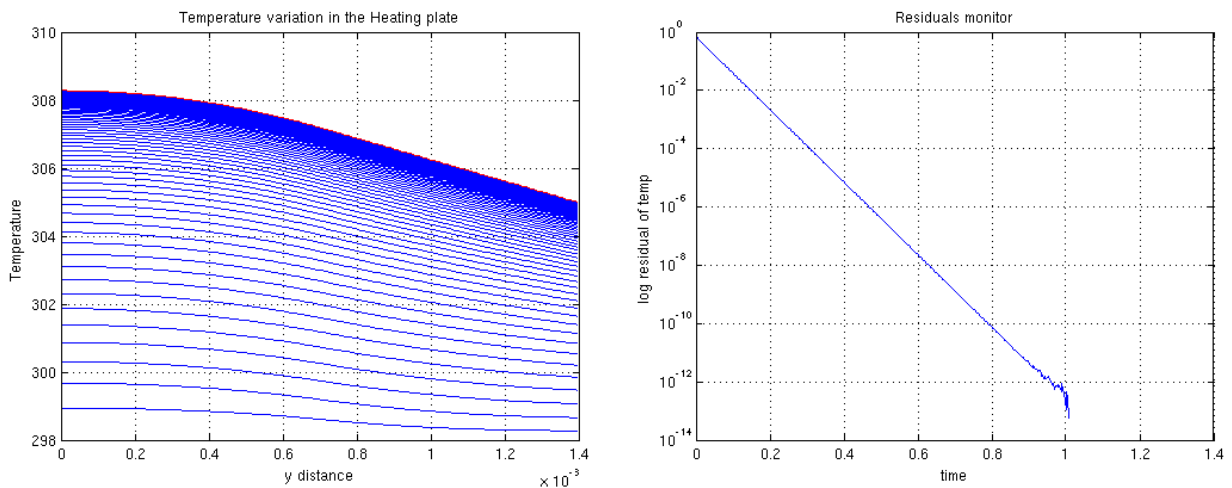

Figure 5.5: *Temperature and convergence study for system with Neumann-Neumann case*

A a grid convergence and time-step convergence study has been performed. A minimum of 5 cells is sufficient for obtaining converged results. But on contrary, the the number of time steps required for achieving converged solution is very high in this case. This could be accounted to the nature of boundary conditions imposed on the system. For number of time steps less than 500, the values are out of range by several orders of magnitude.
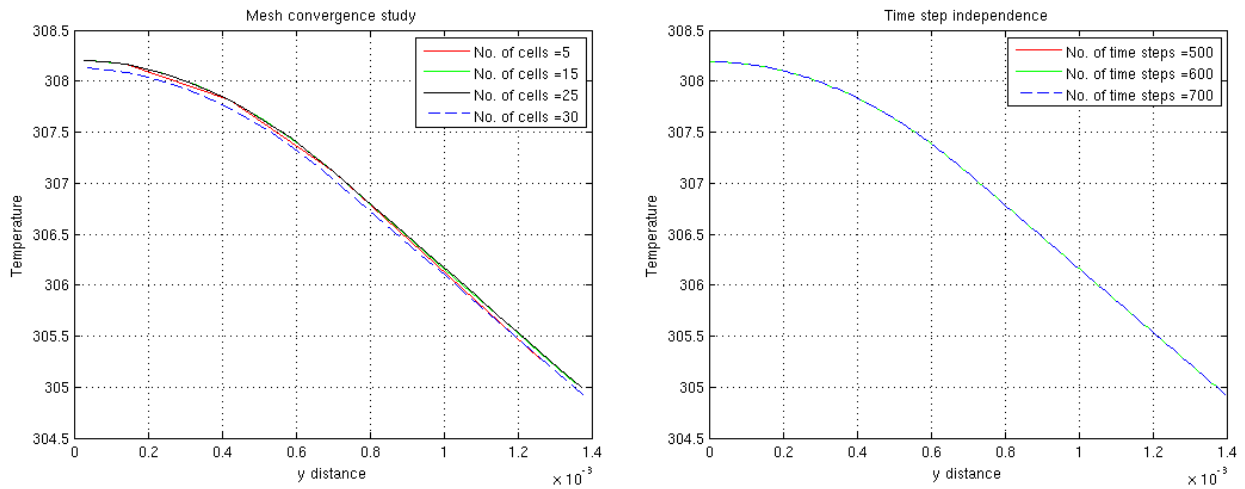
17

Figure 5.6: *Mesh convergence and time step independence study for Neumann-Neumann case*

As the thickness of the plates have been very small, when a Dirichlet boundary condition is set to the boundaries, only a very large value of source term creates an impact. There are two reasons to substantiate this trend. One, for the same volume heat source provided for a thick plate system and a thin plate system, the surface heat flux for the thick plate is higher. Secondly, when a temperature boundary condition is introduced, a higher surface flux to temperature gradient is expected to leave the system when thickness is small. Therefore, to illustrate the impact of source terms in the solver, a thicker domain pertaining to a total length of 1.4m is chosen. Again here, half the domain is set to be occupied by the heating plate made of copper and the rest by the metal substrate made of aluminum. The physical properties remain the same as for the thin plates and the other necessary values used are specified in Table- 5.2
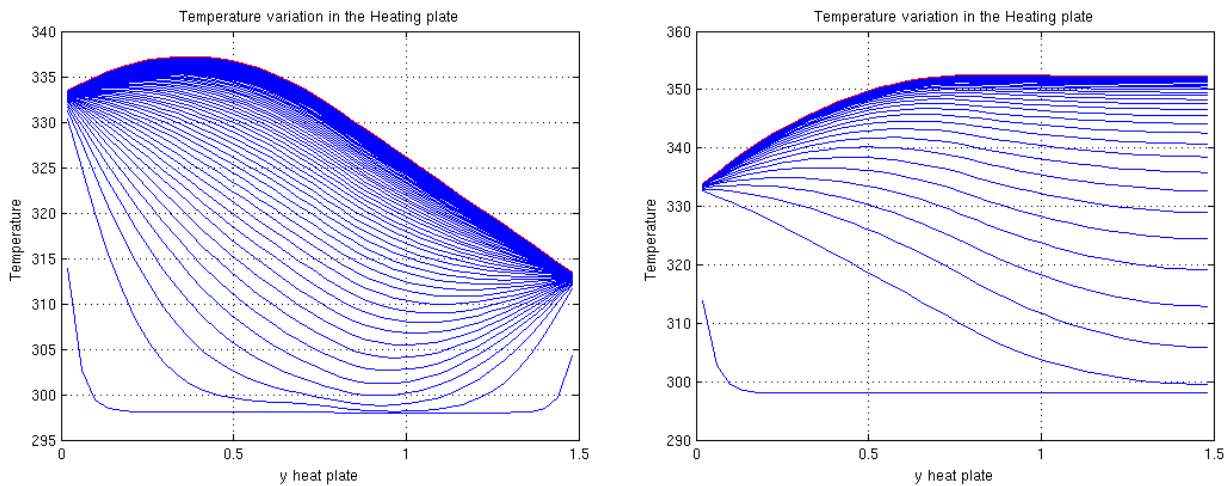

Figure 5.7: *Temperature profiles corresponding to Dirichlet-Dirichlet condition; On the right, temperature profiles corresponding to Dirichlet-Nuemann condition*

As could be seen from the Figure- 5.7, the image on left shows the boundaries assuming the values of the boundary condition and a similar temporal evolution as the previous case with a thin plate system, but in contrast, the steady state value is not a straight line and a rise in temperature in region where source is located. On the right side, the Dirichlet boundary assumes the temperature specified but the steady state temperature is no more the Dirichlet value itself but is increased because of the source. A similar increase in temperature for identical boundary conditions in thin plates would have required very high values of source terms to account for the fluxes leaving the system through the Dirichlet boundary.

Table 5.2: Constants and values; Heat Transfer equation - Thick plates

Physical property/ constants	Values
T_{ref}	298k
Thickness of Aluminum plate	0.75m
Thickness of Copper plate	0.75m
Dirichlet- Dirichlet temperature	333K and 313K
Temperature on Dirichlet-Nueman	333K
Source	25000 W/m^2 (only in the heating plate)

5.2 Mass Transfer Equation for the Paint Layer

The 1-D transient mass transfer equation solved for the study of transport of solvent across and outside the thickness of the paint matrix is the following

$$\frac{DX}{Dt} = \frac{\partial}{\partial x}(D\frac{\partial X}{\partial x}) + \overline{S} \tag{5.18}$$

Similar to the heat transfer equation, the mass transfer was discretized using the FVM approach. The FVM notations followed in the mass transfer equations to specify the spatial and temporal dependence is the same as in the heat transfer equation.

$$\int_{\Delta x}\int_{\Delta t}\frac{\partial X}{\partial t}dxdt + \int_{\Delta x}\int_{\Delta t}V_x\frac{\partial X}{\partial x}dxdt = \int_{\Delta x}\int_{\Delta t}\frac{\partial}{\partial x}(D\frac{\partial X}{\partial x})dxdt + \int_{\Delta x}\int_{\Delta t}Sdxdt \tag{5.19}$$

$$\Delta x(X^1 - X^0) + V_x(X_e - X_w)\Delta t = ((D\frac{\partial X}{\partial x})_e - (D\frac{\partial X}{\partial x})_w)\Delta t + \overline{S}\Delta t \Delta x \tag{5.20}$$

Since the transient 1-D mass transfer equation is solved implicitly, the neighbouring cell concentration values are obtained from the same time step as the simulation has advanced to.

The Peclet Number is defined as the ratio of transport of a property by convection to conduction and since its value is less than unity, the diffusion dominates convection and a discretization scheme that is less diffusive in nature is expected to work good. Therefore, central differencing scheme is used for all the terms in the mass transfer equation. The value of diffusivity D is evaluated by linear interpolation using the distance ratios, as mentioned for the material properties in heat transfer equation.

$$\frac{\Delta x(X^1 - x^0)}{\Delta t} + \frac{V_x}{2}(X_E - X_W) = D_e(\frac{X_E^1 - X_P^1}{\delta x_e}) - D_e(\frac{X_P - X_W^1}{\delta x_w}) + \overline{S}\Delta x \tag{5.21}$$

The mass transfer equation could be represented in general form as the following

$$b_p X_P^1 + b_e X_E^1 + b_w X_W^1 = b_p^0 X_P^0 + C \tag{5.22}$$

The constants are defined as the following

$$b_p^0 = \frac{\Delta x}{\Delta t} ; C = \overline{S}\Delta x \tag{5.23}$$

$$b_e = -(\frac{D_e}{\delta x_e} - \frac{V_x}{2}) ; b_w = -(\frac{D_w}{\delta x_w} + \frac{V_x}{2}) \tag{5.24}$$

$$b_p = b_p^0 + \frac{D_e}{\delta x_e} + \frac{D_w}{\delta x_w} \tag{5.25}$$

The correction of co-efficients for the boundary nodes for the implementation of the implicit boundary conditions have been performed the same way as it was briefed for the heat transfer equation.

Theoretically, reduction of solvent is typically different for different cells, the reduction in height of the individual cells is therefore different. This leads to a varying receding velocity for different cells in the paint matrix. Such evaluation did not lead to any distinct observation in the behaviour of the transport properties as to the one performed by calculating reduction from average concentration reduction. Therefore, the later methodology is adopted for the rest of the work.

In reality, as the amount of solvent present in the ambient air regulates the boundary conditions, i.e if most part of the solvent has already vaporized into air, the diffusion process is slowed down. By actual physics, this process is governed by the partial pressure of solvent in immediate ambient air (partial pressures are proportional to mass fractions), Saturation pressure of solvent in immediate ambient air (describing the amount of solvent the air could accommodate at the maximum), pressure of the paint- air interface and a chemical property of paint (activity of the solvent). But since the solver developed is not coupled with pressure- velocity calculations, the aforementioned values are not feasible to be evaluated. Therefore, an alternative methodology for defining the evaporation of the solvent into the ambient air is performed.

5.2.1 Implicit Boundary Conditions

The availability of experimental measurements provides the opportunity of a flexible modelling of the boundary condition term. The idea of representing the evaporation process as boundary condition is valid as it is a surface phenomenon governed by the interface characteristics. From a mathematical perspective, generalization of the transport behaviour for any paint layer which eliminates the requirement of knowing involved physio-chemical parameters(like the activity of the solvent) is a clear advantage. In the current model, the evaporation rate parameter is assumed to have a linear dependence on the concentration of the solvent in the last computational cell in the paint layer. The concentration flux term is very synonymous to the heat flux term in the heat transfer solver and an analogy on the definition of flux could be drawn as the flux in the heat transfer solver is defined as the following.

$$-k\frac{\partial T}{\partial x} = HTC(\Delta T) \tag{5.26}$$

Similarly, in the mass transfer equation, the the flux is defined as the following

$$-D\frac{\partial C}{\partial x} = Ce_{rate} \tag{5.27}$$

According to the work done by Eres et al[12], the above mentioned formulation of the evaporation parameter rate in the current case would have had the following formulation

$$-D\frac{\partial C}{\partial x} = e_{rate}(1-C)^n \tag{5.28}$$

Here, n is an empirical constant that varied between 0 and 1 based on the concentration of solvent in the reminder of the mixture. However, this formulation is not completely suitable to the current work as a single transport equation is modelled to represent the transport of resin and solvent unlike in the work done by Eres et al[12]. Therefore, it is important to have no sink term once all the solvent in the paint matrix has exhausted. The corrected model used for the purpose is as the following

$$-D\frac{\partial C}{\partial x} = Ce_{rate}(1-C)^n \tag{5.29}$$

The boundary condition on the paint layer- metal substrate interface is fixed to a flux value of 0. This is to ensure that the paint material does not diffuse into the metal substrate.

5.2.2 Verification of Mass Transfer Solver

The Figure-5.11 shows the transport and evolution of concentration of solvent and resin respectively. As described in the Table- 5.3, the initial composition of paint matrix is assumed to be equally contributed by the resin and solvent.

The ends of temporally evolving lines moving closer indicates the reduction in thickness as the composition changes. The figure also shows that the concentration of the solvent has decreased from 0.5 to 0 and the concentration of the resin has increased from 0.5 to unity. This reinforces the physics of the curing process described in the theory chapter that all the solvent must leave the paint matrix and the matrix eventually consists of the irreducible resin component.

The same analysis is also repeated for an initial thickness of 0.0001m too and the impact of initial thickness on the transport behaviour is studied. The major difference is that, the reduced thickness causes a reduction in the time scales of diffusion. Therefore, the reduced concentration of solvent at the air end lowers the

Table 5.3: Constants and values; Mass Transfer Equation

Physical properties/ constants	Values
Paint layer thickness	0.001 m
ρ_{res}	3000 kg/m^3
ρ_{sol}	700 kg/m^3
Temperature	313k
Initial solvent concentration	0.5
Initial resin concentration	0.5
Initial weight	1.12kg
Area of cross-section	1 m^2
e$_{rate}$	700
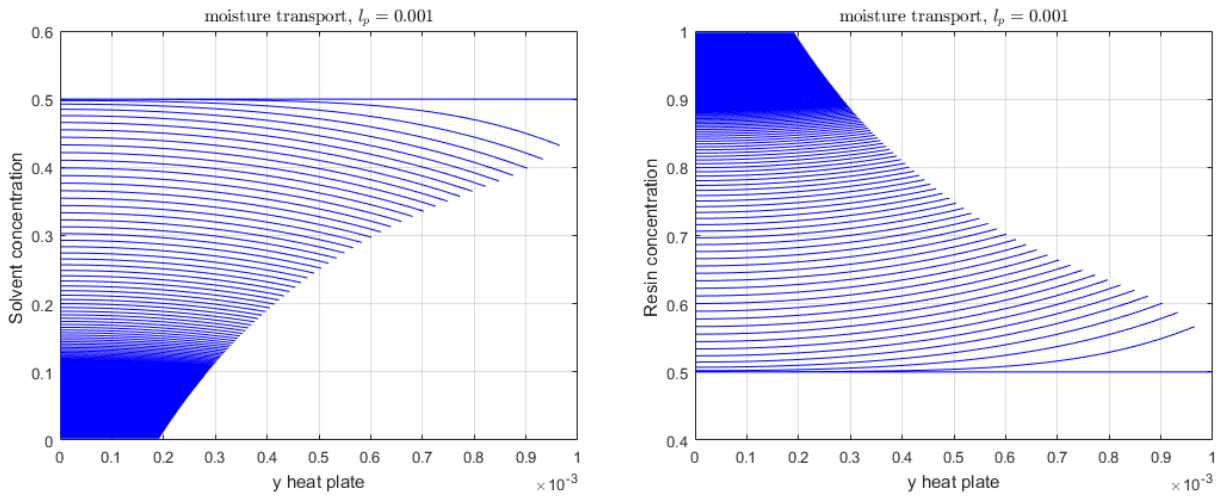
Figure 5.8: *Concentration transport of solvent and resin; The temporal evolution of the composition of the paint matrix as the thickness of the paint layer reduces. These results pertain to an initial thickness of 0.001m*
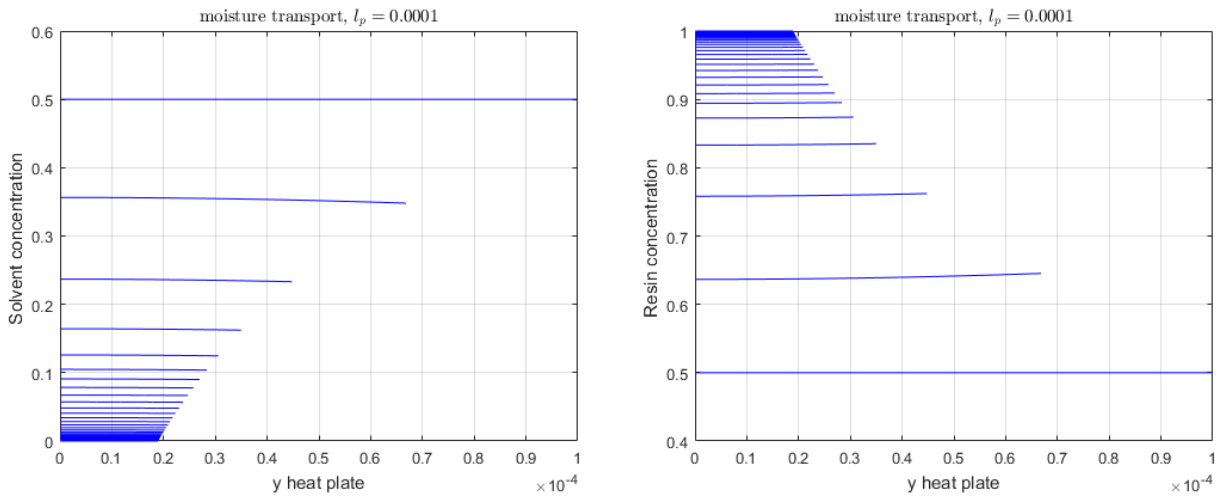

Figure 5.9: *Concentration transport of solvent and resin; The temporal evolution of the composition of the paint matrix as the thickness of the paint layer reduces. These results pertain to an initial thickness of 0.0001m*

concentration at the metal end faster than how the concentration depletes further at the air interface. In a physical standpoint, the impact of a surface phenomena is communicated through the domain faster such that the subsequent change at the surface is preceded by the impact created by the communicated transport

information. This is unlike in the previous case where the increased thickness supported for the presence of a strong concentration gradient. Also, the contour lines indicate that the process has reached steady state much earlier than the thicker counter-part as there are only very less distinct contours indicating the gradient. This is again in consistence with the physics of the problem as one could naturally expect thicker coatings to take more time to get cured.
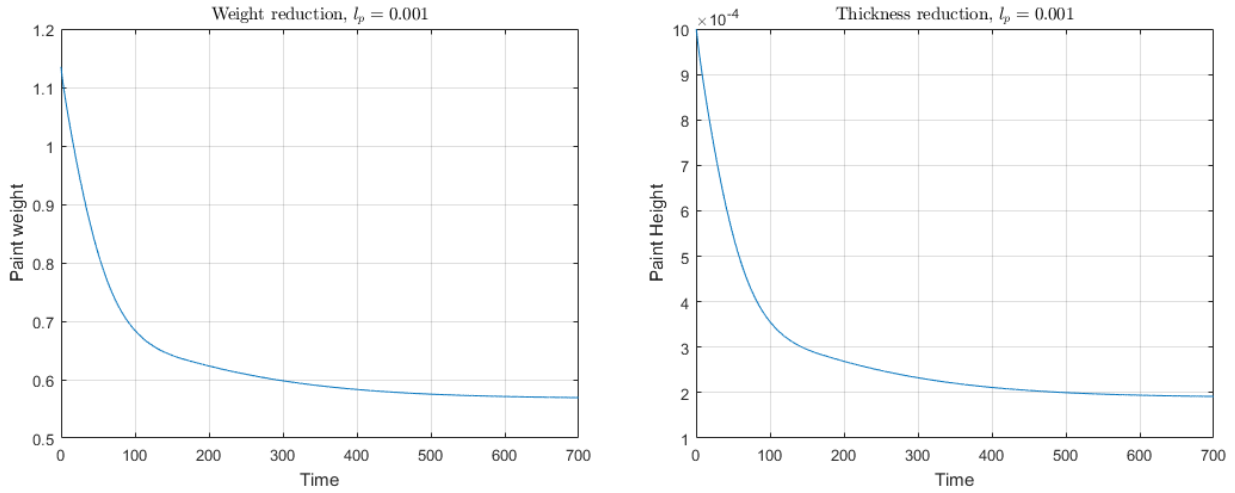

Figure 5.10: *Weight and height reduction paint layer as the paint layer cures; Both shows no further reduction after all the solvent is evaporated out from the matrix*
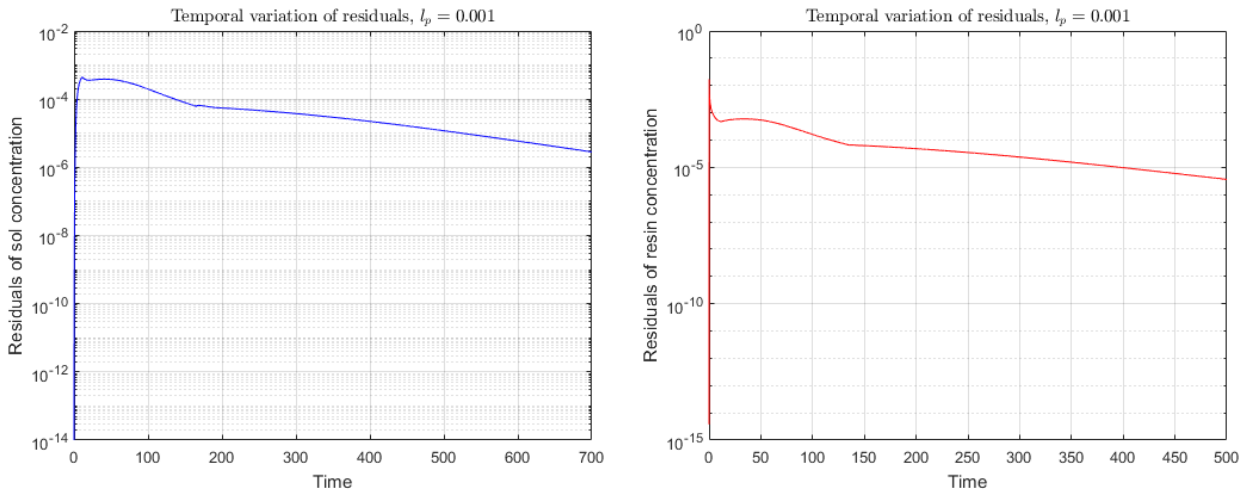

Figure 5.11: *Residuals of solvent and resin concentration as the paint layer cures; The very low residuals indicate a steady state in the composition after all the solvent is evaporated*

As a consequence of the solvent vaporizing out of the paint matrix, the thickness and the weight of the matrix reduces with time. As the mass fractions and the volume fractions could be interchangeably evaluated from the Equation-2.24, initial concentration of 0.5 of both solvent and resin correspond to an initial volume fraction of 0.19 for the resin and 0.81 for the solvent. A reminder thickness of 0.19mm of paint layer thickness from an initially 1mm thick paint layer is hence as discussed in the theory. At this juncture, it is important to note that the evaporation rate parameter is not an evaluated parameter but still an assumed value. Nevertheless, the results developed are representative of the physics of the problem.

It is also interesting to note that the convergence for the residuals of concentration of solvent and resin as seen in Figure- 5.11 are linear. The residuals have been estimated as the maximum difference of concentration observed at any node between the previous and the subsequent time steps and very low value of residuals as

the simulation advances indicates that the composition of the paint matrix has reached a steady state (all the solvent has vaporized into the ambient surroundings.)

It is important to qualitatively understand the impact of the evaporation rate parameter e_{rate} on the amount of solvent evaporating across the paint layer-air interface. Therefore, amount of solvent evaporated across the interface per unit time is compared for a range of e_{rate} values. Also it is of interest to realize the impact of the same on the overall evaporation time and therefore the transient weight of the paint matrix is compared with the same range of e_{rate}.
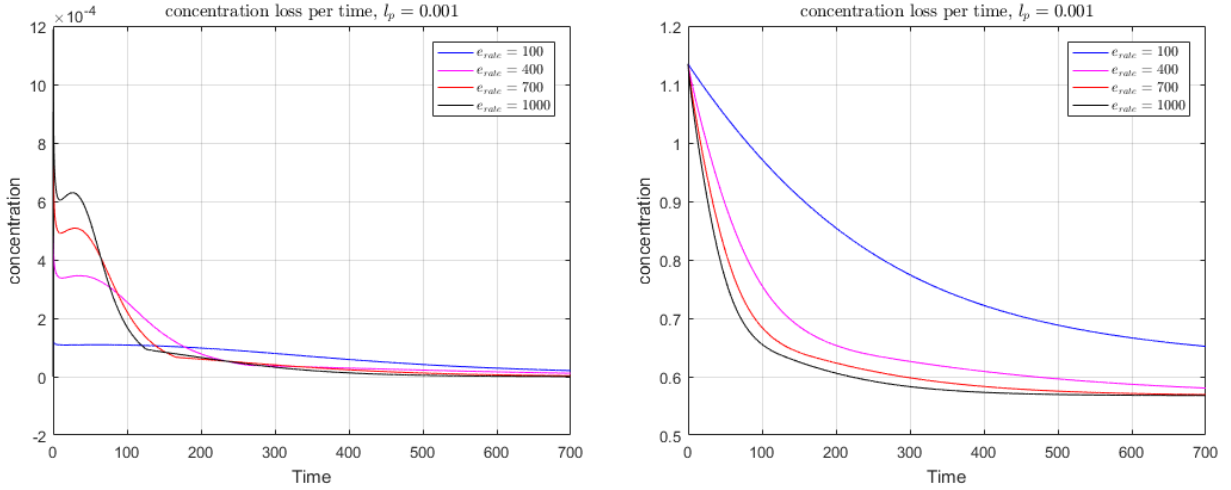

Figure 5.12: *The loss of concentration of solvent across the interface with time is compared for different e_{rate} values; The transient weight of the paint matrix is compared for different e_{rate}*

It is observed from these studies that as a sink like boundary condition term, the larger magnitude of the e_{rate} leads to faster depletion of the concentration of the solvent and the evaporation is completed faster. It is also observed that the peak created by different values of e_{rate} could be representative as well; The higher values of e_{rate} produce larger peaks and shifts the peaks more to the left. This signifies that the instantaneous rate of depletion of solvent concentration per unit time increases and that the overall process is eventually accelerated as well. The nature of results for weight and thickness reduction and residuals study are the same for the reduced initial thickness as well. The very high values of e_{rate} is also representative of how it compensates for diffusivity D when the temperature is as low as 323k and that the entire curing is forced to completion in less than 300s. Therefore, e_{rate} is only representative of the other properties but does not carry physical significance on its own by dimension.

5.2.3   Convergence study for Mass Transfer

Grid convergence study and time step convergence study has been performed for the mass transfer equation with the transient weight reduction and thickness reduction of the paint matrix as the reference parameter. It is observed that the minimum of 5 cells with approximately 400 time steps in necessary for a converged mass diffusion solution in the paint matrix.
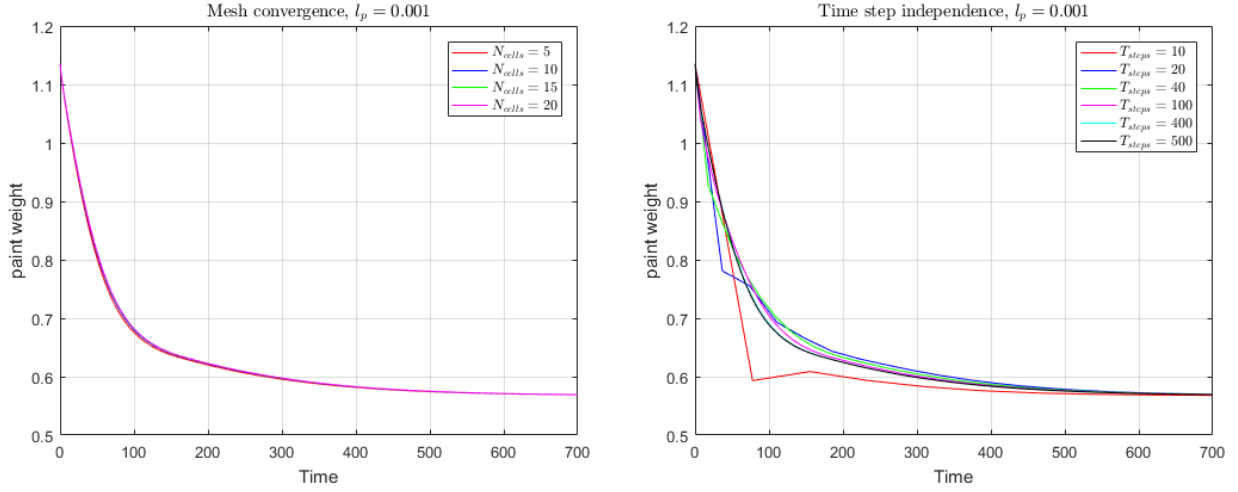
23

Figure 5.13: *The transient weight of the paint matrix is compared for different mesh and time-stepping setups; These results pertain to an initial paint thickness of 0.001m*

The experimental measurements by Swerea-IVF for transient weight reduction has been made for an initial thickness of 0.0001m. Therefore, to substantiate the optimization studies in the coming sections, a mesh convergence and time step independence study is essential to be performed for an initial thickness corresponding to 0.0001m. Also it is necessary to observe the change in requirement of the discretization with the change in initial thickness as the studies in the coming section will involve paint layer of different initial thickness.
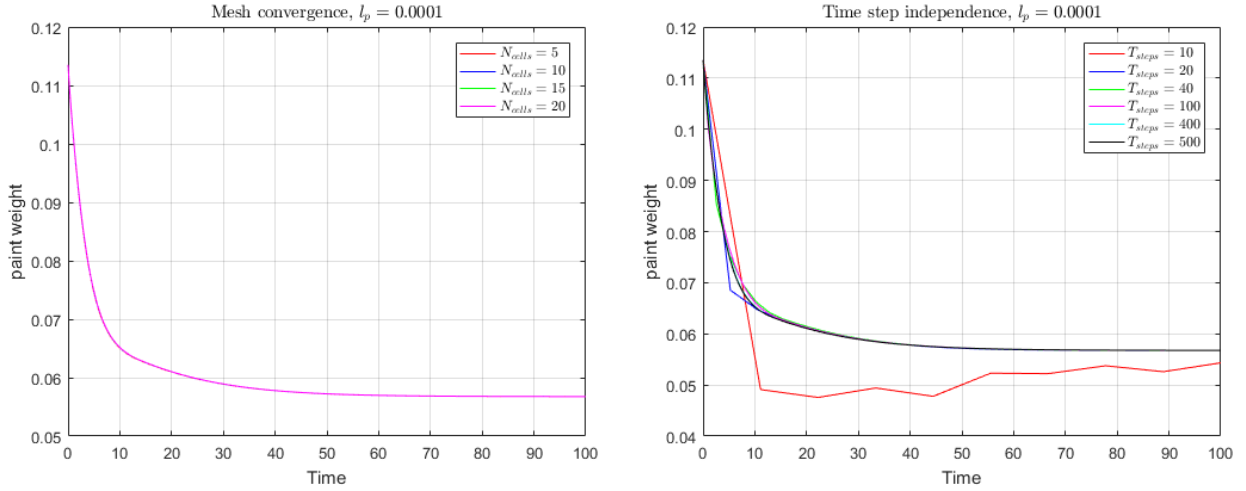

Figure 5.14: *The transient weight of the paint matrix is compared for different mesh and time-stepping setups; These results pertain to an initial paint thickness of 0.0001m*

A minimum of 5 cells and around 400 time steps is found necessary for obtaining convergent solutions. And again around 400 time steps are necessary for the solution to be time step converged.

5.3 Heat and Mass Transfer in the Paint Layer

The aim of this section is to include the study of heat transfer in the paint layer. Previously the heat transfer analysis is performed for the heating plate and the metal substrate. Also the mass transfer analysis is performed with a constant temperature. The mutual dependence of the 1-D mass transfer and 1-D heat transfer equation on each other has to be established. The concentration transport across the paint layer depends on the heat transfer solver as the dffusivity is dependent on the temperature. Unlike for the heat transfer study in the

heating plate and the metal substrate, the heat transfer in the paint layer includes a moving mesh problem and transiently varying material properties. Therefore, the convective term in the material derivative has to be addressed in the heat transfer equation, but only in the domain pertaining to the paint layer. The information regarding both the receding velocity of the mesh and the concentration dependent material properties has to be known based on the solutions from the mass transfer solver.

The concentration dependence of the material properties could be explained as the following.

$$\rho = \rho_{sol}X + \rho_{res}(1 - X) \tag{5.30}$$

$$c_p = c_{p,sol}X + c_{p,res}(1 - X) \tag{5.31}$$

$$\kappa = \kappa_{sol}X + \kappa_{res}(1 - X) \tag{5.32}$$

The mass transfer equation remains the same as what was solved in the previous section. The heat transfer equation solved for in the current study is the following

$$\rho c_p\left(\frac{\partial T}{\partial t} + v_{rec}\frac{\partial T}{\partial x}\right) = \frac{\partial}{\partial x}\left(\kappa\frac{\partial T}{\partial x}\right) + S \tag{5.33}$$

The disretization procedure using FVM for the equations is very similar to the heat and mass transfer equation in the previous studies. From a numerical standpoint, only the computational domain pertaining to paint layer reduces and is hence represented by a deforming mesh. And the computational domain corresponding to metal substrate is irreducible and is hence represented by a non-deforming mesh. The HTC value and the e_{rate} are still assumed values and hence the results are not the final solution only.

The following is the simulation procedure adopted for resolving the heat and mass transport in the paint layer.

- Consider the initial composition of the paint matrix and compute the material properties. Initiate the simulation with $v_{rec} = 0$ in the first time step.

- Solve the heat transfer equation for temperature.

- Evaluate diffusivity and concentration transport.

- Compute weight reduction and thickness reduction and compute the v_{rec}

- Until the end of simulations is reached, go to step two with known v_{rec} and concentration.

The dependence of diffusivity D on the solution of heat transfer solver and the dependence of material properties on the solution of mass transfer solver makes the system strongly two-way coupled. At this juncture, we have clear motivations to perform optimization by inverse simulation techniques. The obvious reason is that the value of HTC and e_{rate} have been assumed and not are not the correct values. The other reason is that the heat transfer equation and the mass transfer equations are completely decoupled. Therefore, it is not assured from the formulation that the heat transfer equation and the mass transfer equation reaches a steady state (dry state) at the same time. Therefore, an optimization procedure is required where the HTC value is optimized with the composition of the paint matrix taken into consideration and e_{rate} with the temperature gradient across the paint layer taken into effect. This optimization process is expected to aid the model parameters HTC and e_{rate} reach a converged value and therefore develop a strong two-way coupling between heat and the mass transfer equation.

The model coupled heat and mass transfer solutions are presented in the following section. This section is not only used to represent and validate the nature of the solver but it also useful in drawing conclusions on ideal simplification that one would like to include in the optimization procedures. The Table -5.4, provides the information on the conditions of the setup, initial and boundary conditions.

25

Table 5.4: Constants and values; Heat and Mass Transfer Equation

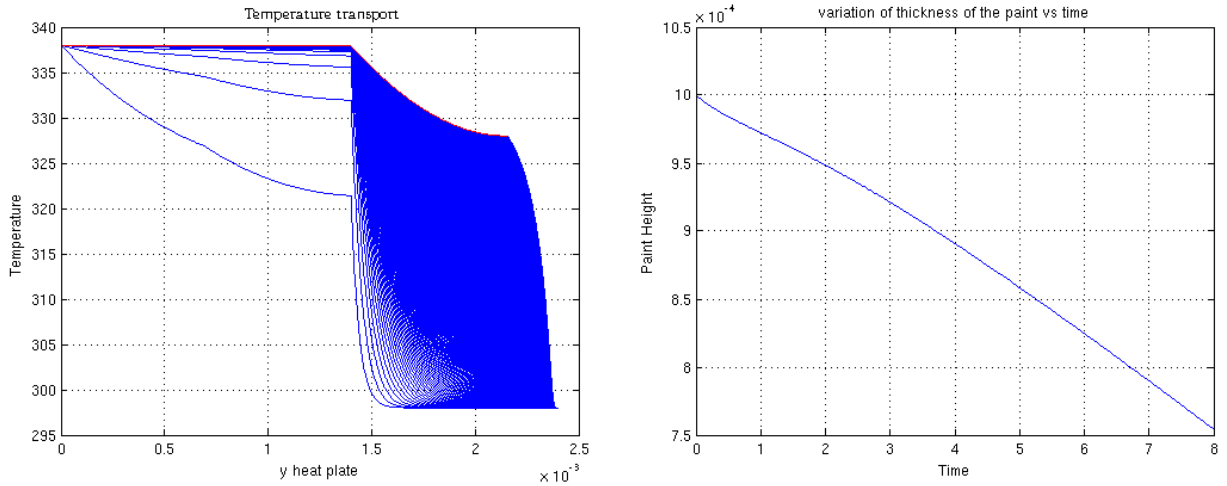| Physical properties/ constants	Values
Paint layer thickness	0.001 m
Thickness of copper plate	0.7 mm
Thickness of aluminum substrate	0.001 mm
ρ_{res}	2664 kg/m^3
ρ_{sol}	1000 kg/m^3
κ_{res}	0.35 W/mk
κ_{sol}	0.606 W/mk
c$_{p,res}$	1000 J/kgK
c$_{p,sol}$	4184 J/kgK
Initial solvent concentration	0.59
Initial resin concentration	0.41
HTC	750 W/m^2K
e$_{rate}$	7000
Area of cross-section	1 m^2
Time	8s
T$_{ref}$	298K

Figure 5.15: *Transient temperature distribution across heating plate, metal surface and paint layer; The figure in the right shows the thickness reduction of the paint layer*

There are some important inferences to deduce from the figure- 5.15. Firstly, the thickness variation suggests that the curing has not reached steady state and for the given duration of evaluation, only less than 20 percent of the thickness is reduced. It is important to note that the given e_{rate} is extremely high. But on the other side, we observe that the gradients are distinctly noticed only in the domain pertaining to the paint material. The domain pertaining to aluminum substrate assumes the temperature of the boundary condition immediately. As mentioned earlier, the solution now incorporates the dynamic change in the physical properties of the paint material as the composition changes and also the reduction in the thickness of the paint could be visualized. The temperature profiles correspond to a reference temperature assumption of 298K.
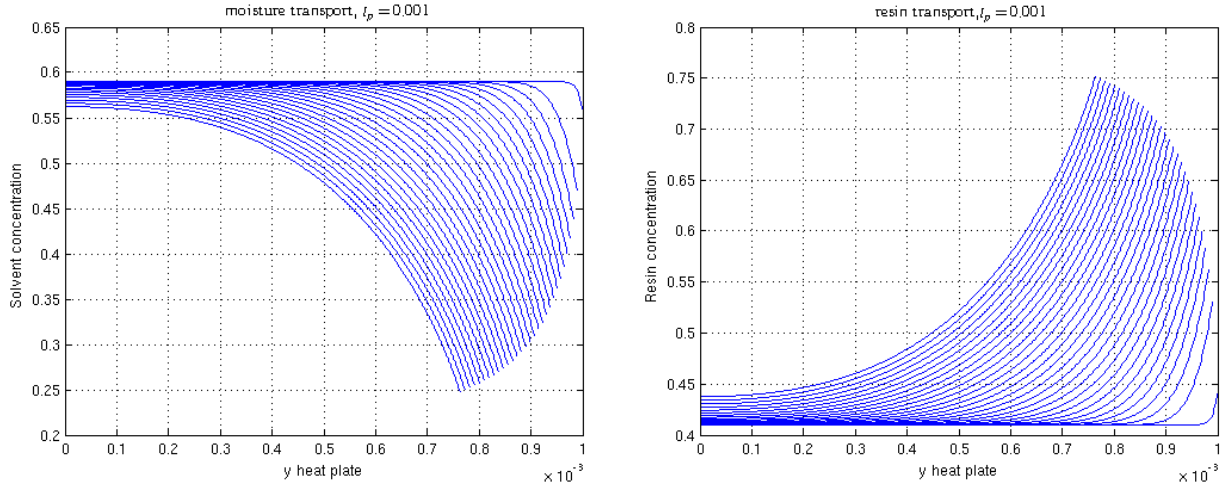
Figure 5.16: *Transient concentration distribution of solvent and resin in combined heat and mass transfer analysis; Here both the resin and solvent concentration are plotted after every 200 time steps.*

As suggested from the height reduction plot in the Figure- 5.15, the Figure -5.16 reinforces the incomplete diffusion of solvent and resin. From the results pertaining to the temperature distribution across the 2 materials and concentration distribution across the paint material, separation of time scales of concentration and heat diffusion in the paint layer with that of the heat diffusion in the metal surfaces is clearly noticed. The separation of scales is observed in-spite of very high choice of e_{rate}, evaporation rate parameter. The usual values of e_{rate} estimated at various temperatures and the time it corresponds for curing were considered prior to the assumption of the same. This was made sure so that the low e_{rate} does not imitate a separation of time scale. This is an expected phenomenon as the conductivity of the metal surfaces are roughly 3 orders of magnitude larger than that of the paint material.

Also it is to be noted that the time scales of heat diffusion has practically very less influence of the HTC. A larger HTC would not suffice to bring the surface sink impact at a rate at which the top of the metal substrate reaches the temperature prescribed for the bottom of the same. This is because of the reason that, convection is a surface property and the less conductivity of the paint material technically makes it a very localized phenomenon. Therefore, before the heat diffusion could communicate the effect of HTC at the metal interface, it is already communicated by the heat diffusion in the metal surface.

A very simple technique to identify an approximate HTC for the system is to perform a static heat balance where the conductive heat fluxes are equated to the convective fluxes as in the Equation- 5.34.

$$q_{conv} = HTC(T_{int} - T_{ref}) = -\kappa\frac{\partial T}{\partial x} \tag{5.34}$$

Here the value of κ is based on an averaged concentration assumption of the paint matrix.

One other consideration for accounting the heat diffusion in the metal surfaces are in the systems where the thickness of the paint layer is thinner than the current assumption. The coupled heat and mass transfer equation was again simulated for the paint layer with a thickness of 0.0001m and HTC value of 7500 W/m^2. The Figure -5.17 indicates that the heat diffusion gradients are seen in the simulation performed for 8s. Also one could observe the change in gradient of temperature loss across a homogeneous metal surface and this expected to be the impact of HTC affecting the metal surface as a consequence of reduced paint layer thickness. Unlike the previous consideration, here the contours are plotted for every time step. This suggests that the major gradients observed are in the first few time steps and after-which they reach the boundary condition value. On the other hand, when the gradients are observed in these first few time steps the concentration gradient developed is not impacting. Perhaps, it should also be noted that the e_{rate} value assumed is so high that in reality, even thinner paint coating layers will take more time to reach the dry state. Therefore, through this analysis, the existence of separation of scales is established irrespective of the thickness of the paint coating.
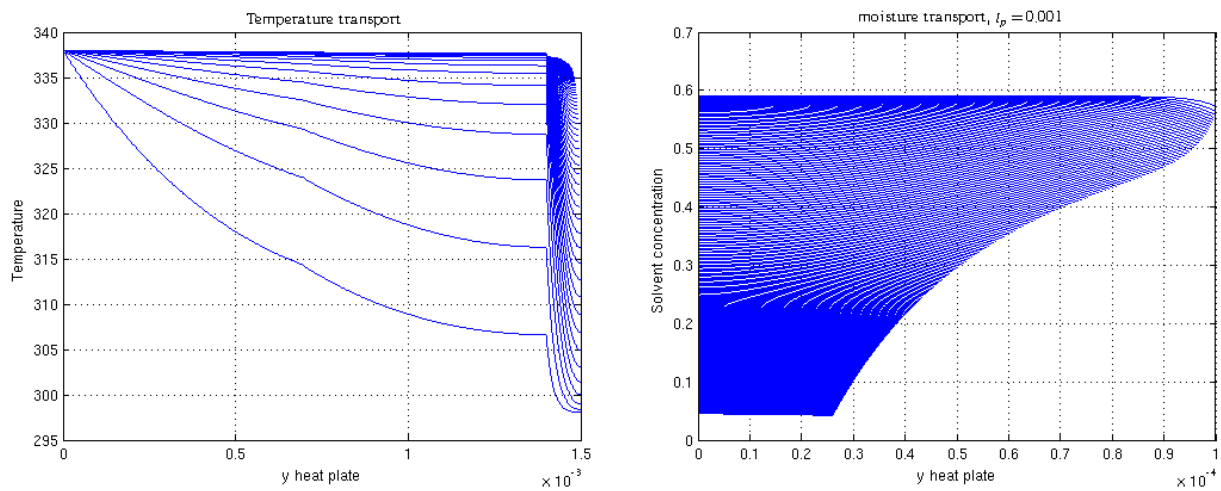
27

Figure 5.17: *Transient concentration distribution of temperature and concentration of solvent in combined heat and mass transfer analysis; Here the contours are plotted at every time instants for both temperature and concentration variations.*

As mentioned in the chapter on experimental measurements, the temperature measurements pertain to the top of the heating plate and top of the paint layer. From the inferences made in the current section, the temperature of the top of the heating plate/ bottom of the metal substrate is assumed to provide the same temperature at the top of the metal substrate without any time difference. This assumption provides ease to the optimization process conducted for the heat transfer where the HTC is estimated with varying concentration.

6   Results and Optimization

The requirement to perform inverse simulations has been detailed in the previous sections. The inverse simulations technique is very instrumental in finding the optimized values of the model parameters, e_{rate}, n_{exp} and HTC in the current study. As illustrated in the chapter on experiments, the experimental measurements of weight reduction of Imron silver and Imron white paints have been performed at 313, 323, 333 and 343K. These experimental measurements have been the reference values for optimization of the e_{rate} and n_{exp} in the mass transfer equation. In regards to previous work in optimization of parameters, reconstruction of parameters of differential equation with noisy data has been implemented by T. Johnson et al[28]. Also the work on multi-parameter optimization has been performed by B. Savioli et al[17] and Jan-Thomas Fischer[24]. In regards to the optimization of HTC from known value of temperatures based on least square approach that incorporates at every time step the impact of optimization parameter on the future time steps is implemented by M. Raudensky [23]. This analysis includes a prior knowledge of thermal conductivity of the material. On contrary, the work by C. Yang et al. included the estimation of thermal conductivity from known transient variation of temperatures across a 1-D domain [30].

In the current optimization process, a simple least square approach is implemented to identify the particular e_{rate} and n_{exp} that produces minimum cumulative error over all the time steps with respect to the experimental measurements. Two different variants have been implemented with the same principle of optimization; single parameter optimization and two- parameters optimization. It is therefore an expectation to verify if the two-parameters optimization is able to produce better agreement with the experimental measurements compared to the single parameter optimization. Also it is to be verified if the two-parameter optimization is a sufficient model in terms of accuracy of the results and the results of the same aid in a scientific decision of whether the adopted model suffices the requirement or if more representative models are necessary for the same. Inverse simulations are solved for e_{rate} in single parameter optimization and e_{rate} and n_{exp} for two parameters optimization. In a physical standpoint, the optimized values of e_{rate} and n_{exp} forces the behaviour of the transport properties to replicate the reality/ experimental measurements which otherwise is done through knowledge of pressure distributions across the paint layer interface and the physio-chemical properties of the paint coating. The aim is to find a constant value for these parameters which represents the physics of the entire problem. At this stage it is to be noted that the solving of the mass transfer is an intermediate step and not the final result it self, and therefore one has the flexibility of modelling source terms. This is unlike the situation for heat transfer equations where the HTC is the final result sought for. The optimized values of n_{exp} and e_{rate} correspond to the chosen model of the source term and is finally expected to agree to the experimental measurements and therefore the concentration values that would be input to the heat transfer equations are still valid.

As mentioned already, the optimization parameters are defined as a function of temperature for a particular paint material.

$$e_{rate} = F(T) \tag{6.1}$$

$$n_{exp} = F(T) \tag{6.2}$$

A primary objective of the entire work, as mentioned in the theory section, is the characterization of HTC with varying composition of the paint and temperature. A decision on whether HTC could be defined using one single parameter corresponding to all the concentrations is appropriate is a requirement. This simplification would largely benefit the 3-D simulations whilst implementing the full scale curing simulations in real time ovens.

The resulted reduced weight because of every value in the range is evaluated for each time step and the value providing absolute cumulative minimum deviation from the reference experimental measurements is regarded as the constant optimized values of n_{exp} and e_{rate} for all the corresponding time steps. Given that $w_{exp,t}$ and $w_{num,i,t}$ are the experimentally measured weight of the paint matrix and numerically evaluated reduced weight at any time instant t, the e_{rate} is principally defined as the following for single parameter and two- parameters optimization

$$e_{rate} = e_{rate} \left(min \sqrt{\sum_{i=1}^{N} (w_{exp,t} - w_{num,i,t})^2} \right) \tag{6.3}$$

$$(e_{rate}, n_{exp}) = e_{rate}, n_{exp} \left(min \sqrt{\sum_{i=1}^{N} ((w_{exp,t} - w_{num,i,t})^2}\right) \qquad (6.4)$$

Here N represents the number of time steps.

6.1 General Algorithm- Optimization process

- Consider the curves of temperature measurements in the Figure- 2.1 as evaluated by thermo-camera. Perform a simple heat balance assuming all the heat flux from the bottom of the paint material to the top of the paint material is converted to convective heat flux. Obtain this value by utilizing the mean values of the initial and final states of the paint during the curing process. As seen in the Figure -2.1, the initial difference in the temperature is significantly very large and correction to allowing only a maximum difference of 30K is to be prescribed.

- The thickness corresponding to the temperature measurements and weight reductions are different and therefore the temperature profiles vary. Define Neumann boundary condition at the paint layer-air interface using the estimated HTC value. Define Dirichlet boundary of 313, 323, 333 and 343K for the 4 different cases at the paint layer-metal interface. Obtain the temperature profile across the thickness of the paint coating.

- Initialize a range for e_{rate}. Evaluate the weight reduction by all the values in the range and determine the value of e_{rate} (in case of single parameter) and e_{rate} and n_{exp} (in case of two- parameters optimization) by evaluating the values of the same for which produces minimum cumulative error over all the time steps. These temporal evaluations of the composition of the paint corresponds to the temperature distribution estimated in the previous step.

- Estimate the value of HTC as performed previously and observe the difference. The procedure is to be continued theoretically so that the estimated value of HTC reaches a converged value.

6.2 Inverse simulations Procedure-

As mentioned in section on coupled heat and mass transfer equations, the material properties of the paint vary as the composition changes as in the Equations 5.30, 5.31 and 5.32. On performing the simple heat balance for heat fluxes across the paint layer as in the Equation -5.34. Therefore for the Imron white paint, the HTC by this technique resulted a value of 50258.919 W/m^2K and 20367.300 W/m^2K at the initial wet and dry state respectively. An average value of 3531.3109 W/m^2K is hence chosen as the first estimate of the HTC value.

This is typically the initiation for the optimization of parameters involved in the mass transfer equations. As mentioned in the earlier sections, the impact of the initialization of the temperature is realized through the diffusivity term. The initialization has therefore made the solving more realistic by introducing a temperature gradient across the paint layer where the composition is evaluated. This procedure where the HTC is obtained in the system pertaining temperature measurements applied in the system pertaining to weight reductions signifies the functional independence of HTC on the thickness of the paint layer. The Figure -6.1 and 6.2, represent the time evolution of temperature (thereby developing a gradient) across the thickness of the paint layer. The significant difference in the temperature across the thickness is also indicative of relatively accelerated mass diffusion in certain regions. This might not be observed very evidently in the results pertaining to mass transfer equation as the boundary condition is very strong and therefore higher concentration diffusion is observed in the paint layer- air interface.
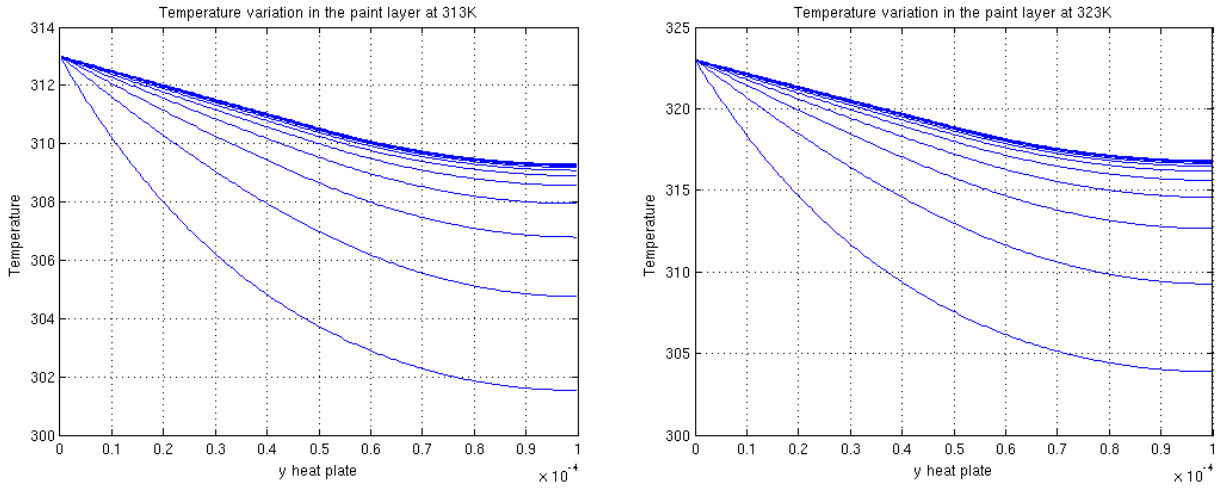
Figure 6.1: *Temperature evolution with Neumann condition defined by HTC value on paint layer-air interface and a Dirichlet condition of 313K and 323K respectively on the metal interface*
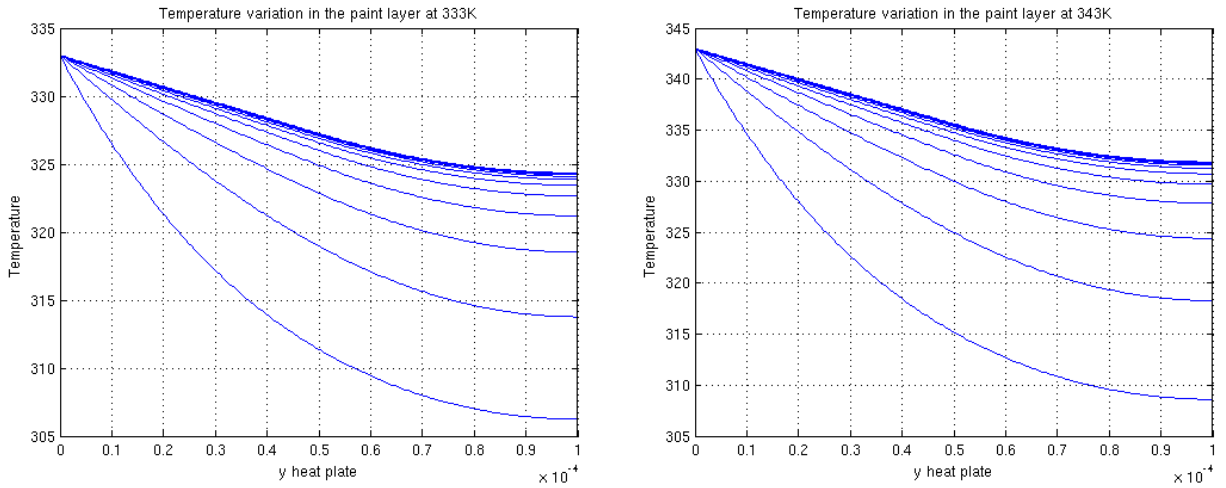

Figure 6.2: *Temperature evolution with Neumann condition defined by HTC value on paint layer-air interface and a Dirichlet condition of 333K and 343K respectively on the metal interface*

6.2.1 One parameter optimization

The temperature profile estimated is the input for this step. For the sake of simplification, the temporal variation of the temperature over the thickness is not considered and just the steady state value is considered. In this single parameter optimization, e_{rate} is the parameter to be optimized. A range of values has to be assigned to e_{rate} and transient weight reduction due to each of these parameters is seen in the Figures -6.3 and 6.4. Aforementioned procedure to estimate the e_{rate} is employed and optimized value is estimated. The Figures -6.5 and 6.6 represents the conformance of numerical predictions of transient weight reduction with experimental measurements at 4 different temperatures corresponding to the values computed by the range of values in the Figures -6.3 and 6.4.
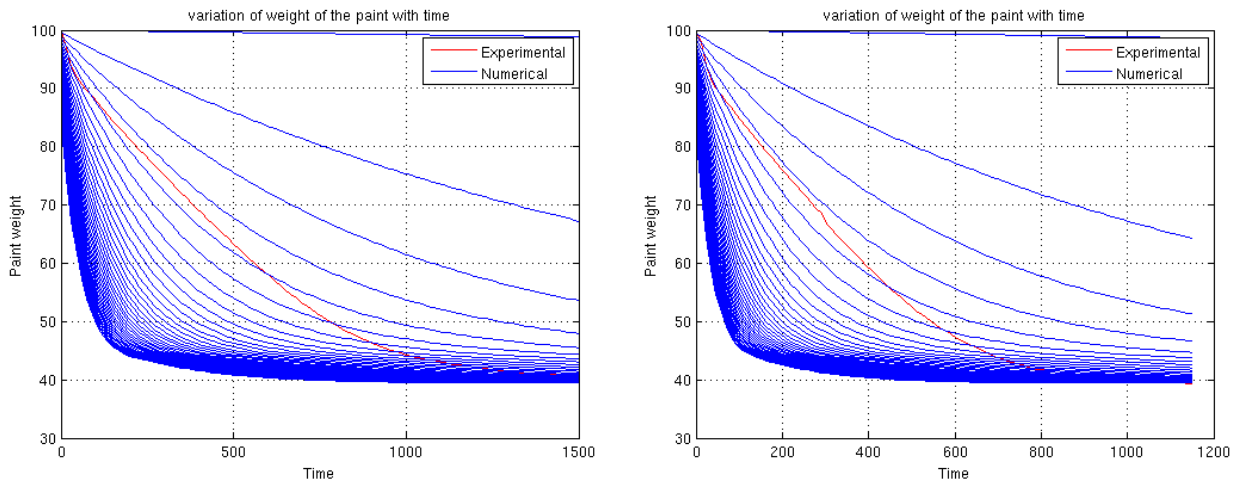
31

Figure 6.3: *Resulting temporal weight reduction at 313K and 323K metal temperature by all the individual e_{rate} values in the range*
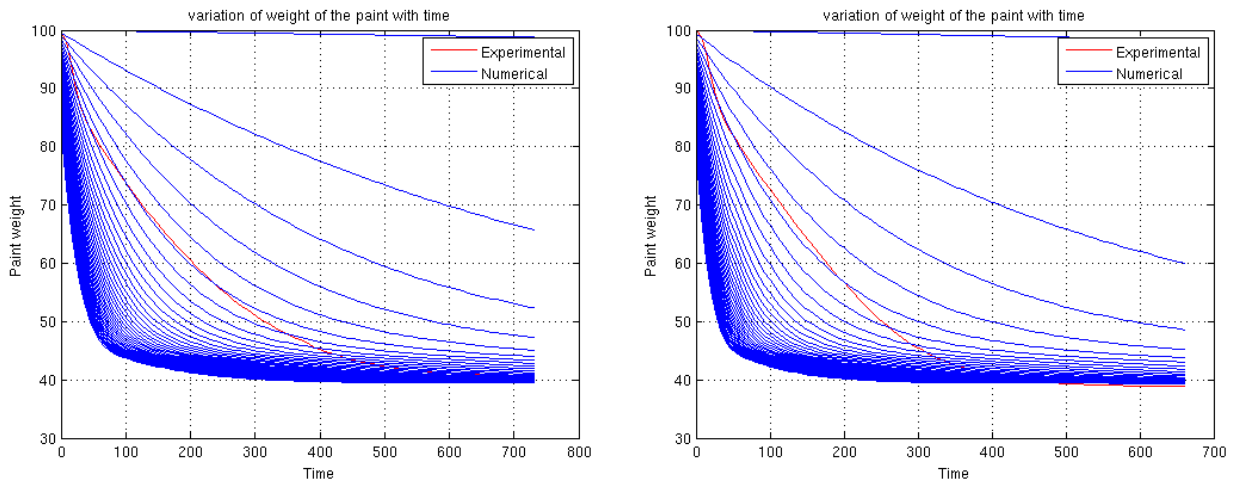

Figure 6.4: *Resulting temporal weight reduction at 333K and 343K metal temperature by all the individual e_{rate} values in the range*

As seen in the Figures -6.5 and 6.6, the overall conformance of the numerical predictions with the experimental measurements is good. The agreement is characteristically very good at the beginning and in the intermediate stages of the curing process and is relatively poor at the end of the curing process. This could be accounted to the definition of the diffusivity model which is incapable of forcing the diffusion process as the concentration of the solvent reduces in the paint matrix. This phenomenon is also characterized by incomplete transient diffusion of the solvent and resin. The Figure -6.7 is the corresponding mass diffusion characteristics at 313K and it shows that neither the solvent has completely left the matrix nor consequently the concentration of resin has reached unity.

This problem of poor agreement of transient weight reduction at the end of the curing could be addressed in different ways. On a physical standpoint, conceiving a more realistic model of diffusivity that ensures completion of diffusion process in a specified time could be considered as a solution. In a modelling perspective, the linear fit does not give enough flexibility for a very good agreement and introducing a model with more than one parameter constraints the numerical predictions in closer agreement with the reference experimental measurements, as done in the current study.
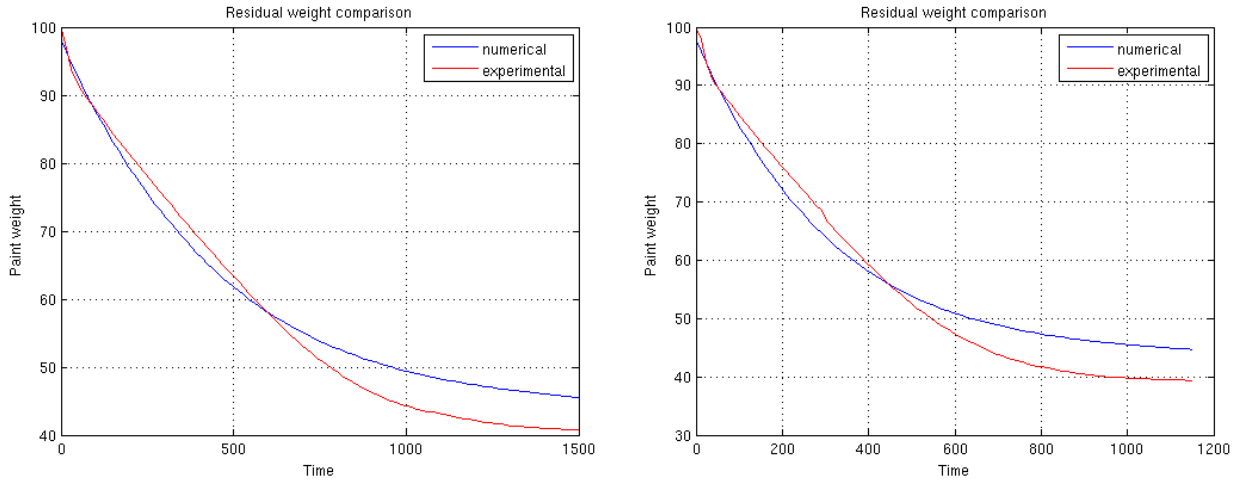
Figure 6.5: *Comparison of numerically estimated weight reduction by optimized value of e_{rate} at 313 and 323K*
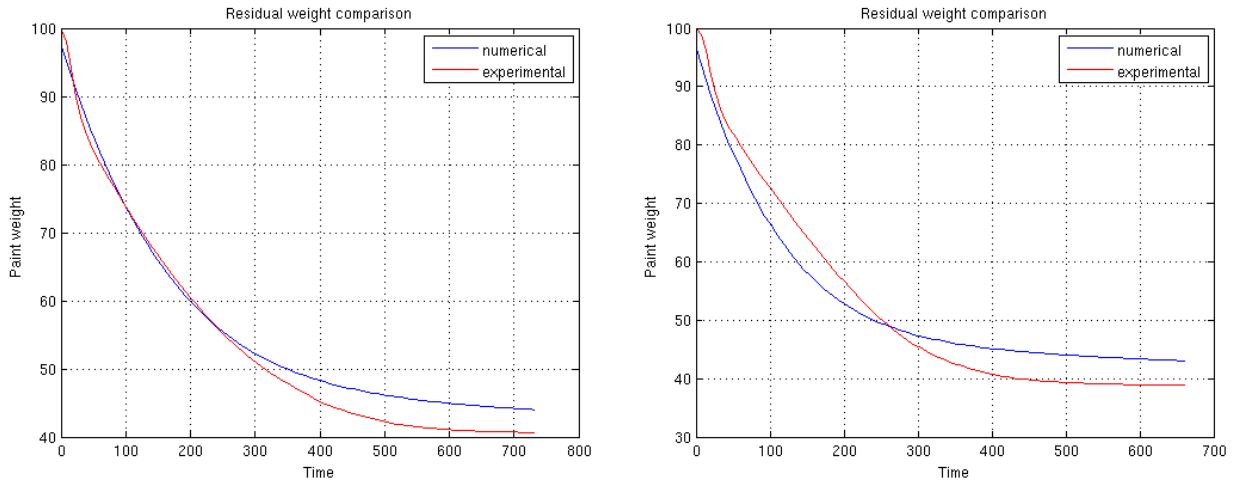

Figure 6.6: *Comparison of numerically estimated weight reduction by optimized value of e_{rate} at 333 and 343K*

Table 6.1: Variation of e_{rate} with temperature

Temperature (K)	e_{rate} value	$\sqrt{\frac{1}{N}(\sum_{i=1}^{N}(w_{exp,t} - w_{num,i,t})^2)}$
313	8.25	3.6745
323	8.25	4.1621
333	10.30	2.7161
343	10.30	4.2928

A similar analysis was also aimed to be performed for Imron silver, but as seen from the Table -4.2, the composition of the paint layer as estimated by the experimental measurements indicate to vary quite significantly as much as by around 5-6 percent in a temperature span of 30K. Also unlike the Imron white paint, the Imron silver paint shows a characteristic trend of depleting resin proportion with increasing temperature and this is against the theory conceived at the beginning of the work as that the composition of the paint is an intrinsic quality of the paint itself. Therefore, further studies pertaining to Imron silver is recommended to carried out after a thorough verification of the experimental results and revisiting of the theory to recognize the influence of temperature on the composition of the paint material. Consequently, the optimization procedure developed

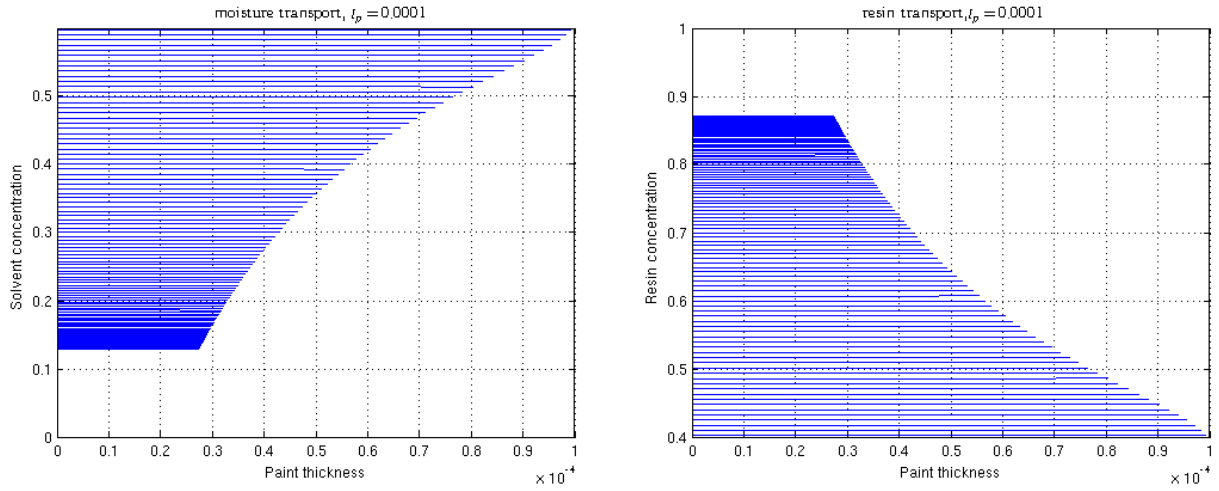using single and two parameters is applied for only Imron white paint material.

Figure 6.7: *Solvent and resin diffusion in time frame frame equivalent to experimental measurements pertaining to boundary temperature at metal interface maintained at 313K*

As intermediate results that help in the estimation of the HTC in the heat transfer solver, the optimized values of e_{rate} at different boundary temperatures have been mentioned in the Table -6.1.

6.2.2 Two parameters optimization

The input to this model is same as for the previous one, which is the temperature profile of the steady state condition. Here a combination of optimized values of e_{rate} and n_{exp} are sought to be estimated. The inputs have been utilized similarly and as expected, the agreement of the numerical predictions have been improved drastically near the dry state of the curing. This technique introduces flexibility in slope of the numerically modelled weight reduction curve. The impact of e_{rate} and n_{exp} in combination at all time steps is seen in the Figures -6.8 and 6.9
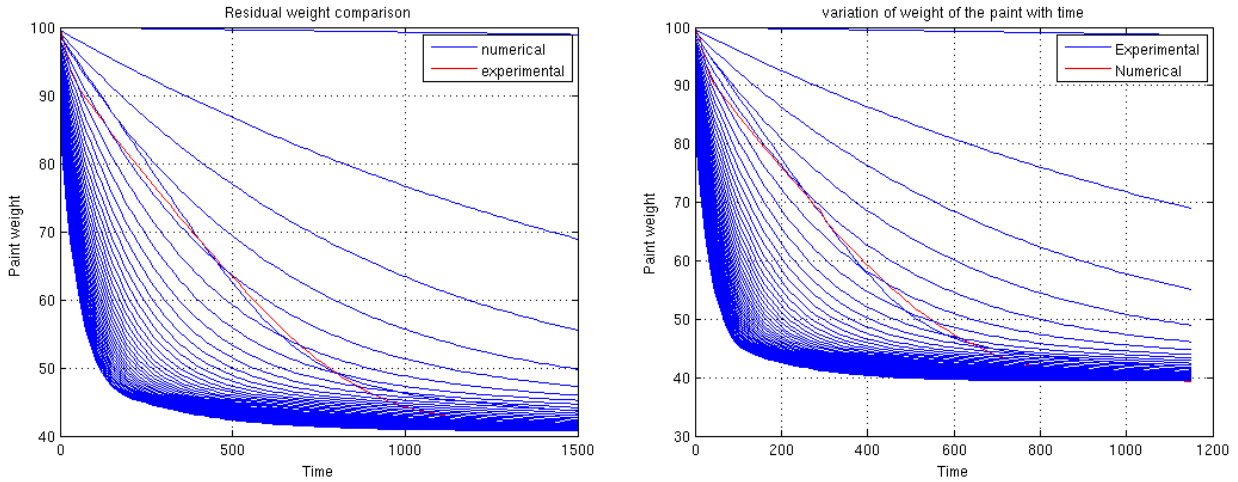

Figure 6.8: *Weight reduction resulted by all the values in the specified range for combination of n_{exp} and e_{rate} at 313K and 323K*
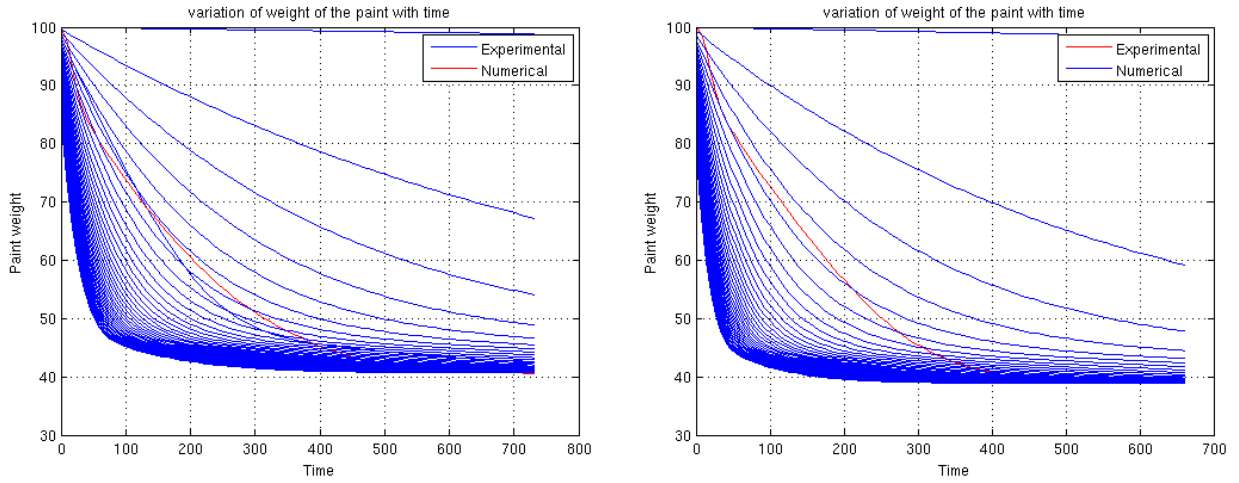
34

Figure 6.9: *Weight reduction resulted by all the values in the specified range for combination of n_{exp} and e_{rate} at 333K and 343K*

As seen in the Figures -6.10 and 6.11, there is a significant improvement in the agreement. The combination of values thus obtained by a similar estimation for single parameter optimization are mentioned in the Table -6.2. Also as seen from the Tables- 6.1 and 6.2, the normalized values of deviation of numerical predictions from the experimental measurements have been reduced at all the operating temperatures in the case of two parameters optimization.

Table 6.2: Variation of e_{rate} and n_{exp} with temperature

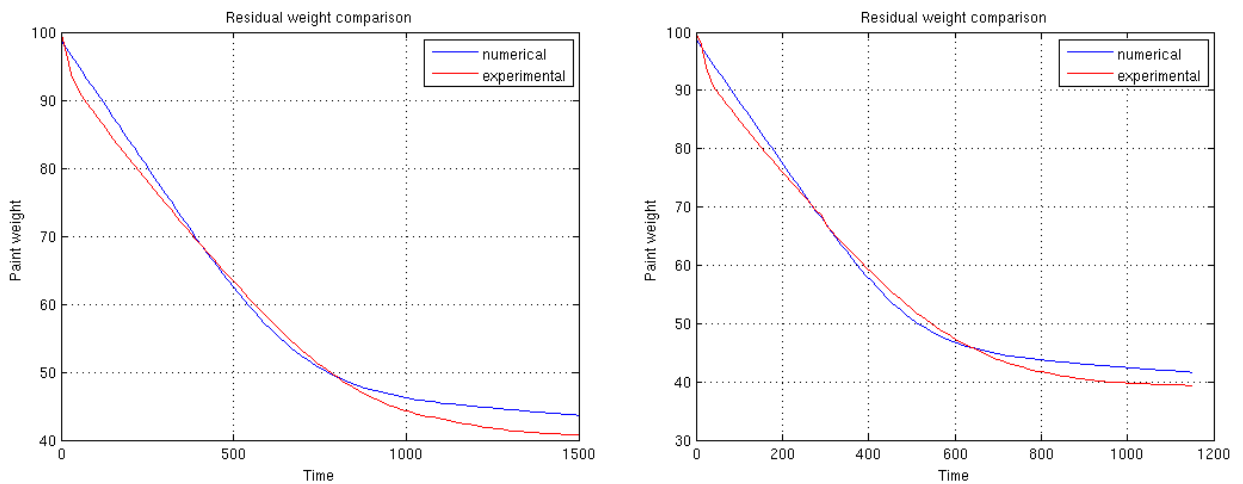| Temperature(K)	e_{rate} value	n_{exp} value	$\sqrt{\frac{1}{N}(\sum_{i=1}^{N}(w_{exp,t} - w_{num,i,t})^2)}$
313	32.85	2	2.1347
323	31.05	2	2.0165
333	32.85	1.556	2.3032
343	32.85	2	2.0878

Figure 6.10: *Comparison of numerically estimated weight reduction by optimized value of e_{rate} and n_{exp} at 313 and 323K*
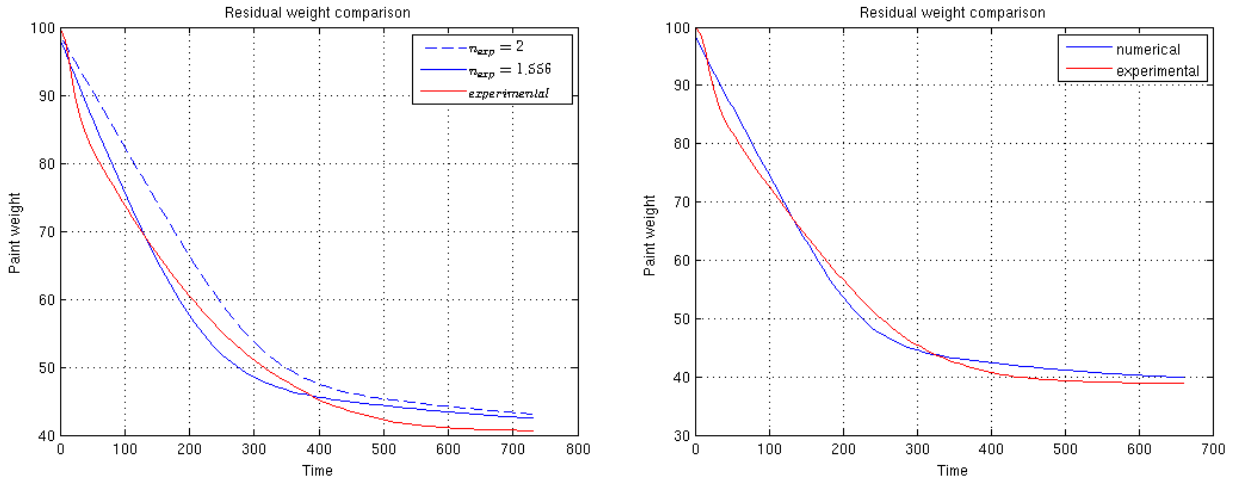
35

Figure 6.11: *Comparison of numerically estimated weight reduction by optimized value of e_{rate} and n_{exp} at 333 and 343K*

Similarly, the Figure -6.12 shows the mass diffusion of the solvent and resin and as seen, the diffusion process is complete and the hence the concentration of the solvent has depleted to almost 0 and the resin concentration has nearly reached unity. This temporal evolution of mass diffusion pertains to boundary temperature of 333K at the metal interface.
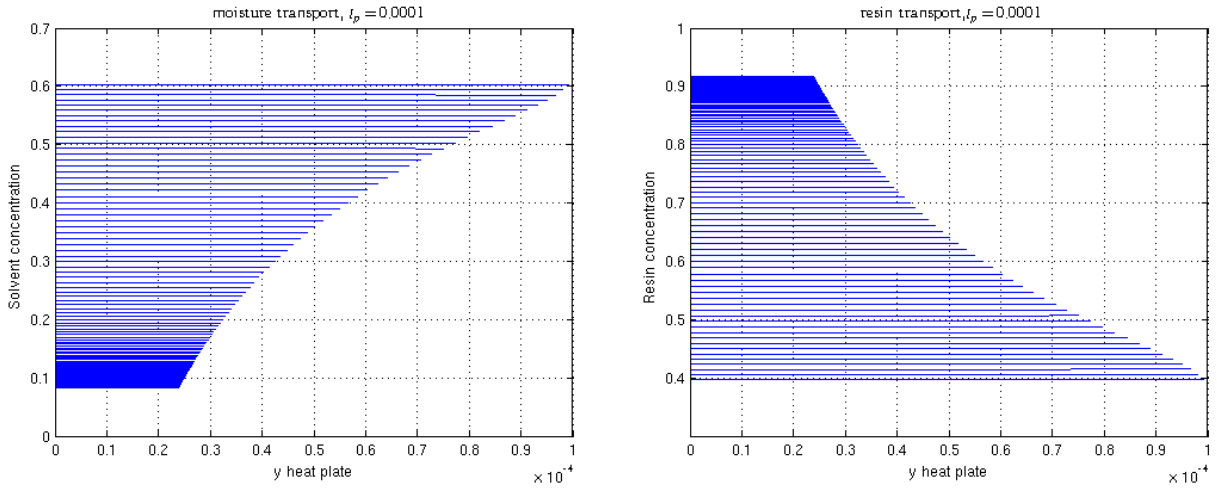

Figure 6.12: *Temporal mass diffusion of solvent and resin pertaining to optimized values of e_{rate} and n_{exp} evaluated at 333K at the boundary with metal substrate*

6.3 Verification of inverse simulations

As mentioned previously, the thickness corresponding to the experiments pertaining to temperature measurements and transient weight reduction measurements are different. As a first step in the iterative optimization solver, the optimized mass transfer equations have been solved and numerical predictions have been matched with the experimental values. This is performed with the assumption that both convective heat sink and convective mass sinks are a surface phenomenon and hence are not dependent on the thickness of the paint coating. Therefore in an attempt to verify this, the optimized e_{rate} value in the case of single parameter optimization and e_{rate} and n_{exp} in the case of two parameters optimization have been forced to define the implicit boundary condition term for comparing the curing time for the paint coating corresponding to the thickness used in the temperature measurements. In the case of optimization with two parameter, the exception

of n_{exp} assuming a different value at 333K is neglected and the most frequently assumed value as a result of optimization is used for the verification. The drying time thus estimated at an average temperature of the paint coating is verified against the experimental measurements.
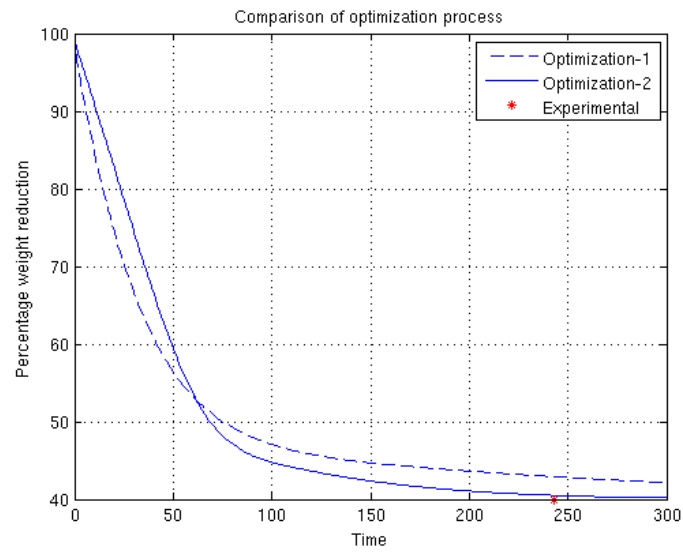

Figure 6.13: *Comparison of drying time as estimated by optimization with single parameter and two parameters*

7 Conclusion and Future Work

7.1 Conclusions

The FVM numerical technique is adopted in the work. At first, 1-D transient heat transfer solver is established for heating plate and metal substrate and the validity of the solver is verified with a variety of boundary conditions. As a part of the forward simulations with heat transfer solver, mesh convergence and time step Independence were established for numerical conformance of solutions from different boundary conditions and to gain pre-processing knowledge for further forward simulations involving simultaneous evaluation of heat and mass transfer solvers and for optimization process involving the inverse simulations. The mass diffusion of solvent and resin were established and the transport of the same were observed to be in conformance with the theory described. Mesh convergence and time step independence study for the mass transfer equations were performed for similar benefits. During this exercise, diffusivity D was found to be incapable of forcing all the solvent out of the paint matrix and it became very less in value with reduced solvent concentration. Therefore, to have a practically short duration for the simulations, a correction was provided to the definition of D which worked with a maximum of 10 per cent error of solvent concentration. To analyze the heat transfer in the paint layer, the evaluation of coupled simulations of 1-D heat transfer equation itself and the 1-D mass transfer equation was realized necessary. Therefore, a domain consisting of non-deformable mesh pertaining to metal substrate and heating plate and a deformable moving mesh pertaining to the paint layer attached to the former mesh was developed. A strong two-way coupling was established where the diffusivity in the paint was defined by the operating temperature in the paint and the material properties characterizing the heat transfer in the paint were defined by the composition of the paint. From the results of 1-D coupled heat and mass transfer equations, a clear separation of time scales were observed between the mass diffusion in paint layer and heat diffusion in the metal surfaces. Having established the representative model results, the exact results required actual values of HTC and e_{rate} and being provided with experimental measurements from Swerea-IVF, the opportunity to benefit from inverse simulations was recognized.

The experimental measurements provided transient weight reduction information for Imron silver and Imron white performed at 313, 323, 333 and 343K. Also temperature measurements were provided for the both where the temperature at the top of the paint layer and the bottom of the metal surface were measured by using a thermocamera. The optimization was first initiated by generating the temperature gradient resulting as a consequence of the HTC. The HTC estimated by heat balance from the setup corresponding to the temperature measurements is utilized for the setup corresponding to weight reduction setups. This could be done with an assumption that the HTC is predominantly affected by the intrinsic characteristics of the paint material. The inverse simulations for the weight reductions were performed with two different source term-like formulations. The flexibility of choosing the source term is a consequence of the requirement that the HTC itself is the final deliverable from the 1-D simulations and neither is e_{rate} nor is n_{exp}. These are applied as implicit boundary conditions to the mass transfer systems and their applicability as boundary conditions are valid as evaporative mass transfer is a surface phenomenon. Since these boundary conditions lead to depleting concentration of the solvent, the higher values of e_{rate} pertained to faster drying and vice-versa for lower values of e_{rate}. In order to estimate the values of e_{rate} and n_{exp}, the least square principle was applied where the absolute error at the individual time steps because of each of the assumed values in the range is cumulatively compared and the ones pertaining to minimum are regarded as the optimized values of e_{rate} in single parameter optimization and e_{rate} and n_{exp} in two parameters optimization. It is observed that the e_{rate} value increased with increasing temperature in the case of optimization with a single parameter and remained constant for all the four operating temperatures for optimization with two parameters. The n_{exp} remained a constant value of 2 for cases pertaining to 313, 323 and 343K respectively. The minimum errors corresponding to two parameters as seen from the Tables -6.1 and 6.2, are very significantly lesser than that for the single parameter optimization. The forced simulation with $n_{exp} = 2$ and $e_{rate} = 32.85$for two parameter optimization at 333K has produced a minimum error that is more than the minimum error produced by single parameter optimization. This is deviant from the expectations and the anomaly at a specific temperature is recommended to be further investigated. This was considered as a motivation for the assumption that n_{exp} is invariant with temperature for the verification of inverse simulations where the weight reduction was estimated by the optimized values. A reasonable agreement provided of the drying time was obtained from the numerical predictions as compared to the experimental measurements. However, one has to consider that this comparison is applicable to only the final point and is a temporal comparison. Perhaps, the given improvement in the agreement of the results by

the suggested methods is one of the ways and since the curing process is a very complex problem involving many parameters, it could aimed to be improved by improving any given independent model, Diffusivity D for example.

7.2 Recommendation for future work

One has to note that the optimization process has just been initiated and not the final results have been achieved. For achieving converged values of parameters, temporally varying gradients of temperature for evaluating mass diffusion and temporally varying concentration gradients for evaluating the temperature need to be established. This process is iterative where the parameters pertaining mass transfer solver are preserved whilst optimizing HTC with heat transfer solver and vice-versa for the mass transfer solver. This process is expected to provide a convergence for the optimization process on a high level and thereby a cascading convergence effect on the optimization parameters as well. Therefore, iteration of optimization process for converged values of parameters is an essential step before the implementation of 3-D simulations.

A more realistic model for the diffusivity is recommended to be researched for and used as the correction provided a very crude fix to force the solvent to leave the paint matrix. As result of the correction, the accuracy lost in the implementation is not accounted and hence a more quantifiable correction to the existing model or a new model itself is expected to be more suitable to the current work.

Also verification of experimental measurements is highly recommended, as the composition measurements from Imron silver had significant deviations in the measurements and also that there is a peculiar deviation of the value of n_{exp} for 333K alone for two parameters optimization. Also more sample measurements would provide conformance to the statistical deviations of the measurements and also a conformance to the limits of variation allowed for numerical predictions as well.

References

[1] Mark A. and van Wachem B. "Derivation and validation of a novel implicit second order accurate immersed boundary method". In: *Journal of computational physics* (). DOI: 227(13):6660-6680(2008).

[2] Mark A. et al. "SIMULATION OF ELECTROSTATIC ROTARY BELL SPRAY PAINTING IN AUTO-MOTIVE PAINT SHOPS". In: *Atomization and Sprays* 23.1 (2013), pp. 25–45. ISSN: 1044-5110.

[3] Nelson K. Akafuah et al. "Evolution of the Automotive Body Coating Process—A Review". In: *Coatings* 6.2 (2016). ISSN: 2079-6412. DOI: 10.3390/coatings6020024. URL: http://www.mdpi.com/2079-6412/6/2/24.

[4] Jochum Beetsma. "Alkyd emulsion paints: properties, challenges and solutions". In: *Pigment & Resin Technology* 27.1 (1998), pp. 12–19. DOI: 10.1108/03699429810194401. eprint: https://doi.org/10.1108/03699429810194401. URL: https://doi.org/10.1108/03699429810194401.

[5] D. BLANC et al. "STUDY AND MODELLING OF COATED CAR PAINTING FILM BY INFRARED OR CONVECTIVE DRYING". In: *Drying Technology* 15.9 (1997), pp. 2303–2323. DOI: 10.1080/07373939708917363. eprint: https://doi.org/10.1080/07373939708917363. URL: https://doi.org/10.1080/07373939708917363.

[6] Thijs Defraeye. "Advanced computational modelling for drying processes – A review". In: *Applied Energy* 131 (2014), pp. 323–344. ISSN: 0306-2619. DOI: https://doi.org/10.1016/j.apenergy.2014.06.027. URL: http://www.sciencedirect.com/science/article/pii/S0306261914006096.

[7] Axalta coating systems Deutschland Co. KG. "Technical Data Sheet basecoat". English. Version Version 2.2.x. In: ().

[8] Axalta coating systems Deutschland Co. KG. "Technical Data Sheet, Imron Hydrobasecoat 8100". English. Version Version 2.2.x. In: ().

[9] R.A Dickie et al. "Modeling paint and adhesive cure in automotive applications1This paper was presented at the 212th National Meeting of the American Chemical Society, in the Roy W. Tess Award Symposium in Coatings honoring Prof. John Kinsey Gillham for his outstanding contributions to coatings science and technology.1". In: *Progress in Organic Coatings* 31.3 (1997), pp. 209–216. ISSN: 0300-9440. DOI: https://doi.org/10.1016/S0300-9440(97)00039-8. URL: http://www.sciencedirect.com/science/article/pii/S0300944097000398.

[10] J. Domnick et al. "Investigations of the drying process of a water based paint film for automotive applications". In: *Chemical Engineering and Processing: Process Intensification* 50.5 (2011). Advances in Coating and Drying of Thin Films dedicated to E.U. Schlünder on the occasion of his 80th birthday, pp. 495–502. ISSN: 0255-2701. DOI: https://doi.org/10.1016/j.cep.2010.08.021. URL: http://www.sciencedirect.com/science/article/pii/S025527011000214X.

[11] Fredrik Edelvik et al. "Math-Based Algorithms and Software for Virtual Product Realization Implemented in Automotive Paint Shops". In: *Math for the Digital Factory*. Ed. by Luca Ghezzi, Dietmar Hömberg, and Chantal Landry. Cham: Springer International Publishing, 2017, pp. 231–251. ISBN: 978-3-319-63957-4. DOI: 10.1007/978-3-319-63957-4_11. URL: https://doi.org/10.1007/978-3-319-63957-4_11.

[12] M. H. Eres, D. E. Weidner, and L. W. Schwartz. "Three-Dimensional Direct Numerical Simulation of Surface-Tension-Gradient Effects on the Leveling of an Evaporating Multicomponent Fluid". In: *Langmuir* 15.5 (1999), pp. 1859–1871. DOI: 10.1021/la980414u. eprint: https://doi.org/10.1021/la980414u. URL: https://doi.org/10.1021/la980414u.

[13] Johan Göhl et al. "An immersed boundary based dynamic contact angle framework for handling complex surfaces of mixed wettabilities". In: *International Journal of Multiphase Flow* (2018). ISSN: 0301-9322. DOI: https://doi.org/10.1016/j.ijmultiphaseflow.2018.08.001. URL: http://www.sciencedirect.com/science/article/pii/S0301932217306444.

[14] Johan Göhl et al. "Simulations of 3D bioprinting: predicting bioprintability of nanofibrillar inks". In: *Biofabrication* 10.3 (2018), p. 034105. URL: http://stacks.iop.org/1758-5090/10/i=3/a=034105.

[15] S. D. Howison et al. "A mathematical model for drying paint layers". In: *Journal of Engineering Mathematics* 32.4 (Nov. 1997), pp. 377–394. ISSN: 1573-2703. DOI: 10.1023/A:1004224014291. URL: https://doi.org/10.1023/A:1004224014291.

[16] Livian Ion and J.M. Vergnaud. "Process of drying a polymeric paint by diffusion-evaporation and shrinkage. Determination of the concentration-dependent diffusivity". In: *Polymer Testing* 14.5 (1995), pp. 479–487. ISSN: 0142-9418. DOI: https://doi.org/10.1016/0142-9418(95)00005-D. URL: http://www.sciencedirect.com/science/article/pii/014294189500005D.

[17] Fischer Jan-Thomas et al. *Multivariableparameter optimization for computational snow avalanche simulation*. 2015. DOI: 10.3189/2015JoG14J168.

[18] Tomas Johnson et al. "A finite volume method for electrostatic three species negative corona discharge simulations with application to externally charged powder bells". In: *Journal of Electrostatics* 74 (2015), pp. 27–36. ISSN: 0304-3886. DOI: https://doi.org/10.1016/j.elstat.2014.12.009. URL: http://www.sciencedirect.com/science/article/pii/S0304388614001338.

[19] H. H. Lou and Y. L. Huang. "Integrated Modeling and Simulation for Improved Reactive Drying of Clearcoat". In: *Industrial & Engineering Chemistry Research* 39.2 (2000), pp. 500–507. DOI: 10.1021/ie990171g. eprint: https://doi.org/10.1021/ie990171g. URL: https://doi.org/10.1021/ie990171g.

[20] A. Mark, E. Svenning, and F. Edelvik. "An immersed boundary method for simulation of flow with heat transfer". In: *International Journal of Heat and Mass Transfer* 56.1 (2013), pp. 424–435. ISSN: 0017-9310. DOI: https://doi.org/10.1016/j.ijheatmasstransfer.2012.09.010. URL: http://www.sciencedirect.com/science/article/pii/S0017931012007041.

[21] Andreas Mark, R Rundqvist, and Fredrik Edelvik. "Comparison Between Different Immersed Boundary Conditions for Simulation of Complex Fluid Flows". In: 7 (Sept. 2011), pp. 241–258.

[22] J. R. Pacheco et al. "Numerical Simulations of Heat Transfer and Fluid Flow Problems Using an Immersed-Boundary Finite-Volume Method on NonStaggered Grids". In: *Numerical Heat Transfer, Part B: Fundamentals* 48.1 (2005), pp. 1–24. DOI: 10.1080/10407790590935975. eprint: https://doi.org/10.1080/10407790590935975. URL: https://doi.org/10.1080/10407790590935975.

[23] Miroslav Raudensky. *Heat transfer coefficient estimation by inverse conduction algorithm*. 1993.

[24] Gabriela B. Savioli and M. Susana Bidner. "Comparison of optimization techniques for automatic history matching". In: *Journal of Petroleum Science and Engineering* 12.1 (1994), pp. 25–35. ISSN: 0920-4105. DOI: https://doi.org/10.1016/0920-4105(94)90004-3. URL: http://www.sciencedirect.com/science/article/pii/0920410594900043.

[25] Clifford Schoff. "Surface defects: Diagnosis and cure". In: 71 (Jan. 1999), pp. 56–73.

[26] Frida Svelander et al. "Robust intersection of structured hexahedral meshes and degenerate triangle meshes with volume fraction applications". In: *Numerical Algorithms* 77.4 (Apr. 2018), pp. 1029–1068. ISSN: 1572-9265. DOI: 10.1007/s11075-017-0352-7. URL: https://doi.org/10.1007/s11075-017-0352-7.

[27] Andersson T. et al. "Multiobjective Optimization of a Heat-Sink Design Using the Sandwiching Algorithm and an Immersed Boundary Conjugate Heat Transfer Solver". In: *Journal of Heat Transfer* (May 2018). DOI: 140(10):102002-102002-10.

[28] Johnson T. and Tucker W. "Rigorous parameter reconstruction for differential equations with noisy data". In: *Automatica J. IFAC* (). DOI: 44(9)(2008),2422-2426.

[29] Benjamin Wettervik et al. "A domain decomposition method for three species modeling of multi-electrode negative corona discharge – With applications to electrostatic precipitators". In: *Journal of Electrostatics* 77 (2015), pp. 139–146. ISSN: 0304-3886. DOI: https://doi.org/10.1016/j.elstat.2015.08.004. URL: http://www.sciencedirect.com/science/article/pii/S0304388615300346.

[30] Ching-yu Yang. "A linear inverse model for the temperature-dependent thermal conductivity determination in one-dimensional problems". In: *Applied Mathematical Modelling* 22.1 (1998), pp. 1–9. ISSN: 0307-904X. DOI: https://doi.org/10.1016/S0307-904X(97)00101-7. URL: http://www.sciencedirect.com/science/article/pii/S0307904X97001017.

[31] Yuan Yi et al. "Improving the Curing Cycle Time through the Numerical Modeling of air Flow in Industrial Continuous Convection Ovens". In: 63 (Dec. 2017), pp. 499–504.